

Origin and evolution of hydrogen-rich gas discharges from a hot spring in the eastern coastal area of China



Yinlei Hao^{a,b,c}, Zhonghe Pang^{a,b,c,*}, Jiao Tian^{a,b,c}, Yingchun Wang^d, Zhongping Li^e, Liwu Li^e, Lantian Xing^e

^a Key Laboratory of Shale Gas and Geoengineering, Institute of Geology and Geophysics, Chinese Academy of Sciences, 100029 Beijing, China

^b Innovation Academy for Earth Sciences, Chinese Academy of Sciences, 100029 Beijing, China

^c University of Chinese Academy of Sciences, 100049 Beijing, China

^d State Key Laboratory of Oil and Gas Reservoir Geology and Exploitation, Chengdu University of Technology, 610059 Chengdu, China

^e Key Laboratory of Petroleum Resources Research, Northwest Institute of Eco-Environment and Resources, Chinese Academy of Science, 730000 Lanzhou, China

ARTICLE INFO

Editor: Michael E. Boettcher

Keywords:

Hydrogen

Low-temperature geothermal system

Water-basalt reaction

Microbial fermentation

Hydrogen isotope

ABSTRACT

Unlike the typical low-temperature (< 150 °C) continental geothermal systems usually characterized by high N₂, CH₄ and CO₂ concentrations but a trace H₂ concentration, the sandstone-dominated Jimo hot spring on China's eastern coast exhibits: (1) abnormally high H₂ concentrations (2.4–12.5 vol%) and H₂/CH₄ (up to 46.5); (2) depleted δD-H₂ (−822 to −709‰), comparable to the Kansas hot springs near the Mid-Continent rift system with the most depleted δD-H₂ (−836 to −740‰) recorded in nature; and (3) dramatic gas concentration and isotope ratio variations within an area of 0.2 km². Gas chemistry and H-C-He-Ne isotope ratios are studied with reference to published H₂ isotope data from various systems. The origin of the gas is most likely attributed to: (a) allochthonous abiotic H₂ generated by the reduction of water and oxidation of Fe^{II}-rich pyroxene and olivine (serpentization) in the basalt located 2 km away under near-surface conditions and migration to the deep sandstone reservoir; (b) primary thermogenic CH₄ produced in the sandstone; (c) mixing with a considerable amount of microbial H₂ from shallow fresh and marine sediments; and (d) biotic CH₄ with typical abiotic signatures resulting from isotope exchanges with fluids high in H₂/CH₄ and CO₂/CH₄ ratios. Allochthonous abiotic H₂ in a sandstone-dominated continental geothermal system and massive microbial fermentation-based H₂ production in shallow fresh and residual marine sediments with insignificant but differential consumption activity are highlighted. The published hydrogen isotope ratios for H₂ produced under various natural geological environmental and experimental conditions have been collected systematically to provide a fundamental framework and an initial tool for restricting the dominant origin of H₂.

1. Introduction

Natural H₂ is one of the substances that provide the energetic drive for deep subsurface lithoautotrophic ecosystems (Lin et al., 2005; Amend and Shock, 2001; Klein et al., 2015a), and it is important for the abiotic synthesis of methane and other organic compounds (McCollom et al., 2016; Etiope and Sherwood-Lollar, 2013), the hydrogenation of petroleum and the formation of ore deposits (Coveney et al., 1987). It also offers an effective means for identifying active faults (Sugisaki et al., 1983; Shangguan et al., 2000; Shangguan and Huo, 2002) and revealing the properties and evolution of mass and energy in the deep Earth (Vacquand et al., 2018; Suda et al., 2014; Arnason, 1977). In natural systems, the production and consumption of hydrogen gas are

closely coupled, resulting in very low concentrations (Hoehler et al., 1998). Hydrogen-rich (> 10%) gas discharges in hydrothermal systems are generally found in volcanic zones with high reservoir temperatures (Coveney et al., 1987; Arnason and Sigurgeirsson, 1968), oceanic rift zones (Zolotarev et al., 1978) and serpentinite-hosted geothermal systems associated with ultrabasic or basic rocks (Vacquand et al., 2018; Suda et al., 2014; Proskurowski et al., 2006; Taran et al., 2010; Abrajano et al., 1988; Coveney et al., 1987; Neal and Stanger, 1983) but are usually not significant in low-temperature sedimentary continental geothermal systems (< 150 °C). The latter are generally characterized by high proportions of gases containing nitrogen (N₂), methane (CH₄) and carbon dioxide (CO₂) (Feldbusch et al., 2018).

The Jimo geothermal system with an average reservoir temperature

* Corresponding author at: Institute of Geology and Geophysics, Chinese Academy of Sciences, 100029 Beijing, China.

E-mail address: z.pang@mail.igcas.ac.cn (Z. Pang).

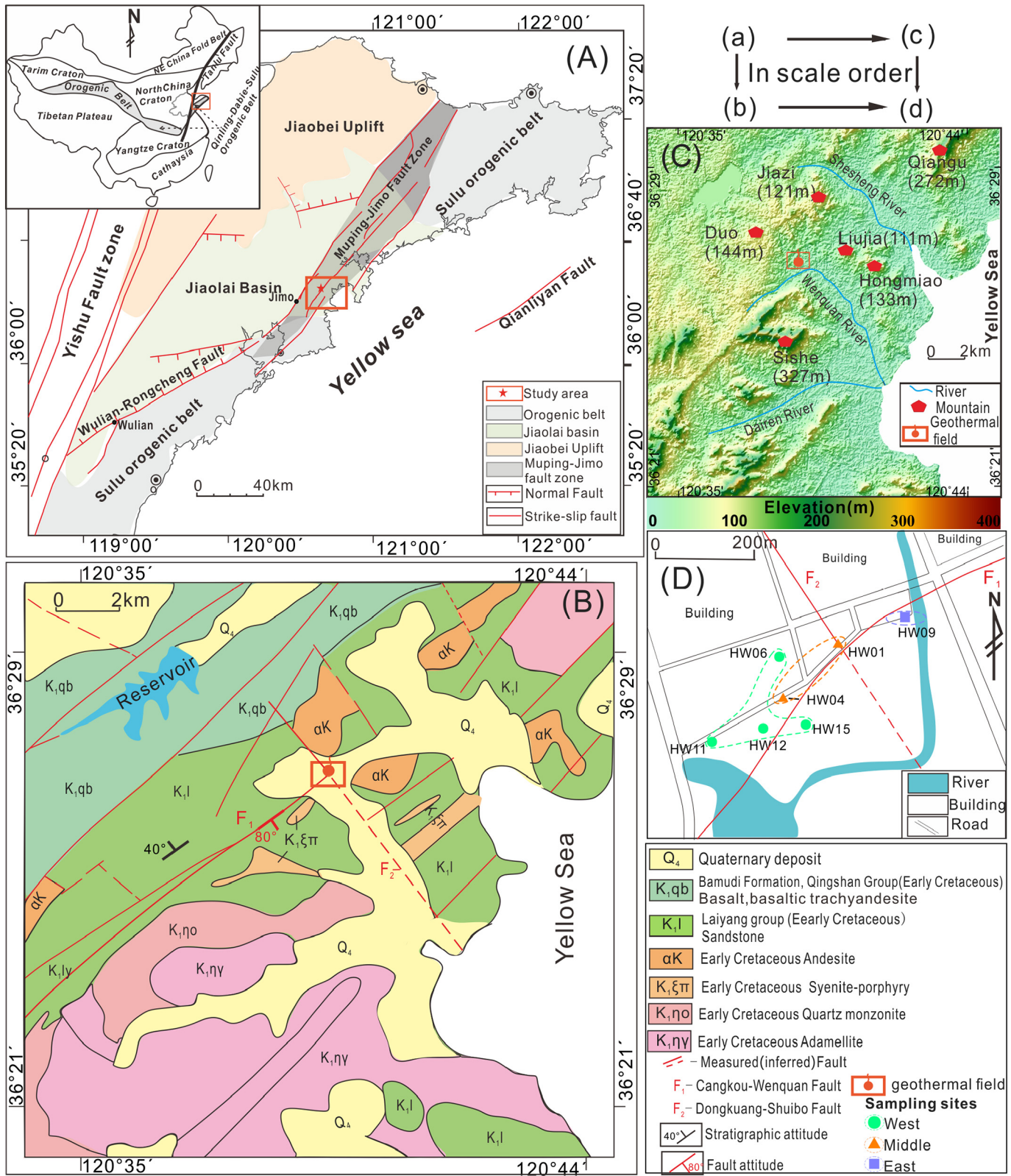


Fig. 1. (A) The tectonic location of the study area modified from Zhang et al. (2019) and Zhang and Sun (2002). (B) A geological sketch map of the study area. (C) A topographical map of the study area. (D) Geothermal water and gas sampling sites.

of 137 °C is an important part of the east coast geothermal zone in China, from the Liaodong and Shandong peninsulas in the North to Fujian and Guangdong in the south, where abundant low temperature (< 150 °C) geothermal systems are located (Kearey and Wei, 1993). Tectonically speaking, the Jimo geothermal field is located in the

Muping-Jimo fault zone, which is a part of the very large Tancheng-Lujiang strike-slip fault system (Tanlu fault zone). The gases from the geothermal systems along the eastern coastal area and the Tanlu fault zone are dominated by crustal gases with low H₂ concentrations (< 0.5%) (Liu et al., 2001; Tao and Liu, 2000; Shangguan et al., 1998;

Yuan, 2013; X. Wang, 2018; Pang, 1987; Feng et al., 2016; Minissale et al., 2008). By contrast, in the Jimo geothermal system there are high concentrations of H₂ (2.4–12.5%) and the lowest δD-H₂ values (−822 to −709‰) found in nature, except in Kansas, where δD-H₂ values of −836 to −740‰ have been determined but occur in a different type of environment (Coveney et al., 1987). The δD values of H₂ in the study area are also lower than that in Mali (−702‰), where there is a large accumulation of natural hydrogen in a similar type of environment with Jimo geothermal system. The accumulation of H₂ in Mali is attributed to the multi overlaid doleritic sills and aquifers preventing upward gas migration and leakage. Hydrogen generation has been suggested to be issued from basement based on the radiogenic helium and argon. But the specific generation mechanism hasn't been proposed (Prinzhofen et al., 2018). Therefore, studying the generation and evolutionary histories of gases, especially abnormal H₂, may provide insights into the geological and tectonic properties within the Earth in the absence of deep drilling.

In addition, the isotope composition of gases has been regarded as less affected by shallow processes and is widely used as tracers to provide information from depth beneath shallow, meteoric-dominated geothermal reservoirs (Lowenstein et al., 2015) and in geothermometry (e.g., H₂O-H₂, CH₄-H₂ and CO₂-CH₄ isotope geothermometers) to estimate deep equilibrium temperatures (Bottinga, 1969; Horibe and Craig, 1995; Arnórsson, 2000). However, dramatic variations in the gas concentrations (e.g., 10% for H₂, 3.5% for CH₄) and isotope composition (e.g., 113‰ for δD-H₂, 207‰ for δD-CH₄) within a limited area of 0.2 km² reflect significant secondary modification processes. To reveal the genetic information from deep-seated resources using gas isotopes, it is necessary to determine the influences of shallow processes on the gas geochemistry and isotope characteristics and to test the applicability of geothermometers under these circumstances. Other than carbon isotopes that are widely documented, systematic analysis of the hydrogen isotopes in H₂, CH₄ and H₂O from samples in nature are rare and have been reported in only a few studies (Suda et al., 2014; Fritz et al., 1992; Proskurowski et al., 2006). Applications of H₂-H₂O and CH₄-H₂O isotope geothermometers are primarily used in high-temperature (> 200 °C) geothermal systems, while limited applications are available in nonvolcanic, low-temperature geothermal systems (Horibe and Craig, 1995; Proskurowski et al., 2006; Suda et al., 2014). In principle, if a full equilibrium is reached, a consistent temperature would be obtained based on the CH₄-H₂O and H₂O-H₂ geothermometers. However, the geochemical and isotope composition of deep-seated geothermal gases flowing up from a deep reservoir can be modified by secondary processes, such as biological activity, redox reactions and re-equilibration, which lead to deviations from concordance as discrepant kinetics of the isotope exchanges in H₂O-H₂ and CH₄-H₂O (Bradley and Summons, 2010). Therefore, deviations from geothermometric agreement can be informative in understanding the evolution of H₂ and the influence of shallow processes.

In the present study, geothermal gas concentrations and isotope composition (³He/⁴He, ⁴He/²⁰Ne, δ¹³C-CO₂, δ¹³C-CH₄, δD-H₂, and δD-CH₄) have been studied, and a systematic synthesis of published hydrogen isotope ratios of H₂ and the isotope fractionation factor between H₂O and H₂ from various systems in nature and experiments have been conducted to (a) unravel the origins and evolutionary histories of gases (especially H₂) in the Jimo hydrothermal system and (b) provide insights into shallow secondary processes that can modify the geochemical and isotope composition of gases.

2. Geological setting

The study area is located in the southeastern Jiaodong Peninsula, which neighbors the Yellow Sea to the east (Fig. 1A). Tectonically, it is a part of the Muping-Jimo fault zone, which is an important part of the giant Tanlu strike-slip fault system and has a length of 200 km and a width of 20–40 km (Zhang et al., 2007; Li et al., 2007). In addition, the

Muping-Jimo fault zone is also a vital tectonic boundary, not only forming the boundary of the North China block and the Sulu orogenic belt combined with the Wulian-Rongcheng fault zone (Zhang and Zhang, 2008) but also controlling the formation and development of the Jiaolai basin (Fig. 1A) (Zhang et al., 2019). The faults in the study area are primarily NE- and NW-trending (Fig. 1B). The dominant NE-trending Cangkou-Wenquan fault is broad in scale and characteristic of tensional activities at early stages and more recent compressional activities. The weak parts of the compressional NE fault provide favorable geothermal pathways and fractured reservoirs (Liu et al., 2009). The NW extensional Dongkuang-Shuibo fault is a water-conducting fault. The Jimo geothermal field is located at the junction of the Cangkou-Wenquan and Dongkuang-Shuibo faults.

The basement in the study area is composed of Archean and Paleoproterozoic metamorphic rocks (Zhou et al., 2016). The strata overlying the basement in unconformity are dominated by Early Cretaceous Laiyang Group (K₁l) clastic rocks and Qingshan Group (K₁q) pyroclastic rocks (Fig. 1b). The K₁l Group is a fluvial-lacustrine sedimentary system that consists of yellow to green sandstones, conglomerates, mudstones, and shales. The K₁q Group is dominated by volcanic and volcanoclastic rocks, which include four eruptive cycles recorded as follows: the Houkuang Formation (K₁qh), Bamudi Formation (K₁qb), Shiquanzhuang Formation (K₁qs), and Fanggezhuang Formation (K₁qf) (Zhang et al., 2016). Among these, the Bamudi Formation (K₁qb) is the most widely distributed and consists of a series of intermediate-basic volcanic rocks including andesite, basaltic andesite, basalt, schönfelsite and basaltic-trachyandesite (Zhang et al., 2016; Qi, 2010; Ji, 2017; Zhu et al., 2012; Wan and Zhang, 1987; Zhang and Sun, 2002). The central zone of the volcanic cycle is located in the Muping-Jimo fault, and the thickest area is > 3000 m in the Jimo area (Zhai, 2003; Li et al., 2007). In the study area, the Bamudi Formation (K₁qb) is primarily located approximately 2 km northwest of the Jimo geothermal system (Fig. 1B). According to previous studies, the Jimo basaltic group erupted at 110–130 Ma and was derived from the partial melting of the metasomatized enriched lithospheric mantle, which has undergone a recent fluid metasomatism by the deeply subducted Yangtze lower/middle crust through tectonic underplating during the formation of the Dabie-Sulu UHP orogen (Fan et al., 2001; Zhang and Sun, 2002). The unconsolidated Quaternary sediments are widely distributed in the geothermal field and run 10–25 m deep. From bottom to top, the types of sediments are Holocene black marine muds, brown lagoon clays and lacustrine silty sediments (Liu et al., 2009).

The study area is surrounded by mountains on three sides with altitudes from 111 to 327 m a.s.l. (Fig. 1C). One hot spring (now dry) and geothermal wells are distributed at the conjunction of the NW and NE faults over an area of 0.2 km² (Fig. 1D). Geothermal wells were drilled to depths from 125 to 245 m, with a maximum yield of 1019 m³/d from a single well. The highest temperature and total dissolved solids (TDS) are up to 89.5 °C and 10.83 g/L (Table 1), respectively. The geothermal waters are dominated by Cl-Na-Ca and Cl-Na types (Hao et al., 2019).

3. Sampling and analysis

The gas and water samples in the study area were collected in July 2017. The locations are shown in Fig. 1D. In total, seven gas samples and seven hot water samples were obtained from the geothermal wells from the western to the eastern parts of the geothermal field.

Sampling was performed after the continuous pumping of the wells for longer than 20 min. The measurement of the temperature, pH, oxidation-reduction potential (ORP) and TDS of the geothermal water were conducted on-site with a portable multiparameter system (HQ40D, Hach). All the water samples were stored in high-density polyethylene bottles. Gas samples were collected by a gas drainage method using lead glass bottles (50 mL) with very low helium permeability. These bottles were initially filled with corresponding geothermal water and submerged into the geothermal water. A cooling coil

Table 1

Temperature, pH, oxidation-reduction potential (ORP) and TDS of the geothermal water and chemical composition of gases (vol%) from the Jimo geothermal system.

Area	Sample ID	Location	Geothermal water				Gas composition (vol%)					
			T(°C)	pH	ORP (mV)	TDS (g/L)	He	H ₂	O ₂	Ar	N ₂	CH ₄
West	HW06	Hongxiang	74.3	7.16	-30.5	2.72	0.04	12.45	2.35	1.02	83.81	0.27
	HW11	Qinglanlan	60.0	7.30	-39.6	2.47	0.02	5.63	6.87	1.44	85.11	0.88
	HW12	Jiedao	70.2	7.11	-27.6	3.61	0.05	7.18	1.30	2.12	87.78	1.28
	HW15	Xianquan	48.2	7.48	-18.3	4.19	0.01	6.83	0.32	2.37	89.44	0.84
Middle	HW01	Lijun	89.5	6.78	-7.1	10.83	0.53	2.38	2.30	2.38	88.56	3.81
	HW04	Hongri	80.0	6.93	-16.4	6.72	0.23	8.69	3.33	1.68	84.34	1.69
East	HW09	Fengquan	60.0	4.19	157.2	8.06	0.09	7.26	1.12	2.02	86.87	0.74

has been connected with the outlet of pipeline (Arnórsson, 2000) and the other end of the cooling coil is connected with a silicon tube for gas collection. After the entire sampling apparatus was purged with geothermal fluids, and a steady flow of gas through the sampling line was attained, the gas was collected by displacement the geothermal fluid in the bottle. Finally, the bottles were sealed with rubber plugs and adhesive plaster, and encapsulated in a 500 mL polyethylene bottle filled with the corresponding geothermal water to avoid atmospheric contamination during transport. During the entire process, no stainless steel vessels were used to eliminate corrosion and H₂ production by geothermal waters reacting with the stainless steel vessels (Sherwood-Lollar et al., 1993; Neal and Stanger, 1983).

The determination of the water isotope ratios (δD and $\delta^{18}\text{O}$) was conducted with a laser absorption water isotope spectrometer analyzer (Picarro L 1102-i) with analytical precisions of 0.1‰ for $\delta^{18}\text{O}$ and 0.5‰ for δD at the Water Isotopes and Water-Rock Interaction Laboratory in the Institute of Geology and Geophysics, Chinese Academy of Sciences.

Gas analysis was performed in the Key Laboratory of Petroleum Resources Research, Institute of Geology and Geophysics, Chinese Academy of Sciences. The chemical composition of gases was determined using a MAT 271 mass spectrometer with a detection limit of 0.0001%, and the relative standard deviations were below 5% (Tian et al., 2018). The determination of the carbon isotopes in CO₂ and CH₄ was performed on a GC-IRMS analytical system gas chromatograph (Agilent 6890) and a stable isotope ratio mass spectrometer (Thermo-Fisher Scientific Delta Plus XP) coupled with an online sample pre-processor (Tian et al., 2018; Zhou et al., 2017). The results are expressed using δ units with respect to the Pee Dee Belemnite (PDB) standard. The measurement errors and analytical precisions were $\pm 0.2\%$ and 0.3% , respectively. The $^3\text{He}/^4\text{He}$ and $^4\text{He}/^{20}\text{Ne}$ ratios were determined with a Noblesse noble gas mass spectrometer (Nu Instruments, UK) calibrated with air from the Gaolan Hill area south of Lanzhou (Tian et al., 2018). The D/H ratios of methane and hydrogen were analyzed for using a MAT 253 (Thermo Fischer) mass spectrometer. The H₂ and CH₄ were separated on a CP-Al₂O₃/KCl chromatographic column (50 m \times 0.53 mm \times 15 μm). The temperature was started at 60 °C for 5 min and ramped up to 200 °C at 15 °C min⁻¹, and this temperature was then maintained for 20 min. The flow rate of high purity helium (99.9999%) as a gas carrier was 3 mL/min. The temperature of the reducing furnace was 1460 °C. The CH₄ working standard gas has a known isotopic composition, namely, $\delta\text{D}_{\text{vsmow}} = -146.0\% \pm 5\%$, which was used as the internal standard to check the stability and accuracy of the instrument during each sample testing process.

4. Results

The results of the on-site measurements on the geothermal waters, determination of dissolved gas concentrations and stable isotope composition for the seven geothermal well waters are presented in Tables 1 and 2.

4.1. Water and gas chemistry

The geothermal waters in the study area within 0.2 km² exhibit a wide range of TDS levels from 2.5 to 10.8 g/L and temperatures (48.2 to 89.5 °C) with a decreasing trend from the central to the western and eastern parts. The opposite trend in the pH and ORP values from the eastern part to the western part reflects the transition from an acid-oxidizing environment (pH = 4.19, ORP = 157 mV) to a weakly alkaline-reducing environment (pH = 7.48, ORP = -18.3 mV).

The major components of the dissolved gases are N₂ (83.8–89.4 vol %) and H₂ (2.4–12.5 vol%), which are significantly distinct from the gases of the other geothermal systems along the eastern coastal area and the Tanlu fault belt that are dominated by N₂, CO₂ or CH₄, with a trace of H₂ (< 0.5%), but they have similar N₂ origins dominated by atmospheric N₂ and sediment-derived N₂ (e.g. release of N₂ from decomposition of organic matter or ammonium in the interspaces of clays) (Fig. S1 of the Supplementary material; Liu et al., 2001; Shangguan et al., 1998; Tao and Liu, 2000). The majority of geothermal samples except for HW11 have O₂ concentrations lower than 5% and N₂/O₂ ratios 23 times higher than the air ratio of 3.73 on the average, reflecting that operational air contamination by sampling problem is insignificant (Tardani et al., 2016). Although high concentration of O₂ (6.87% vol%) for HW11, the N₂/O₂ (12.4) are about 3 times higher than the air ratio, also indicating a limited operational air contamination. N₂/Ar ratio of HW01 is 37.2 close to the value of air-saturated water (ASW = 38.6), suggesting that N₂ is mainly from water previously equilibrated with atmosphere (ASW). The increase trend of N₂/Ar ratios from HW01 to western and eastern parts (37.7–82.2) reflects additional air compositions (AIR = 83.6) or sediment-derived N₂ has been added in the samples western and eastern parts (Fig. S2 of the Supplementary material; Gigganbach and Poreda, 1993).

Three distinct parts of the study area can be identified based on the geographic locations, geochemical characteristics of the geothermal water (temperatures, TDS, pH and ORP), and a reactive (H₂, CH₄, and CO₂) and nonreactive (N₂, He, and Ar) gas composition (Fig. 2).

Central part: The geothermal waters exhibit high temperatures (> 80 °C) with pH values ranging from 6.78 to 6.93 and less negative ORP values (-16.4 to -7.1 mV). In this area, the CH₄ (1.7–3.8 vol%) and He (0.23–0.53 vol%) concentrations are the highest of those from the three areas, while the concentrations of CO₂ (0.04%) and H₂ (2.4–8.7 vol%) are the lowest. Therefore, the highest CH₄/CO₂ (42–95) and lowest H₂/CH₄ (0.6–5.1) values are observed in this part.

Western part: The geothermal waters show relatively low temperatures (48.2–74.3 °C) and a weakly alkaline-reducing environment. The gas mixtures in this area are characterized by the highest H₂ concentrations (5.6–12.5 vol%) and H₂/CH₄ ratios (5.6–46.1).

Eastern part: The environment in this area is acid (pH = 4.19) and oxidizing (ORP = 157 mV). The temperature is similar to that of the geothermal water in the western part. The CO₂ concentration in this area is 7–47 times higher than the concentrations in the western and middle parts, and the CH₄/CO₂ ratio of 0.4 is the lowest.

Table 2

Isotope composition and relative helium contributions from mantle and crust for gas samples in the Jimo geothermal system. R/Ra represents helium isotope ratios normalized to the air isotope Ra = ${}^3\text{He}/{}^4\text{He} = 1.4 \times 10^{-6}$ (Sano and Wakita, 1985).

Area	Sample ID	Location	Helium and Neon Isotopes				Helium ^b contributions (%)	$\delta^{13}\text{C}$ (‰ PDB)		δD (‰ VSMOW)			$\delta^{18}\text{O}$ (‰ VSMOW)	$\alpha^{13}\text{C}_{\text{CH}_4-\text{CO}_2}$	
			${}^3\text{He}/{}^4\text{He}$	${}^4\text{He}/{}^{20}\text{Ne}$	R/Ra	Rc/Ra ^a		Mantle	Crust	CO ₂	CH ₄	H ₂	CH ₄	H ₂ O	
West	HW06	Hongxiang	9.11 E-07	66.0	0.65	0.65	7.9	92.1	-18.5	-39.8	-740.3	-427.8	-51.48	-7.14	0.9783
	HW11	Qinglanlan	7.73 E-07	16.4	0.55	0.54	6.5	93.5	-21.6	-37.5	-773.5	-249.6	-45.79	-6.14	0.9837
	HW12	Jiedao	8.20 E-07	36.8	0.59	0.59	7.1	92.9	-20.2	-41.4	-738.0	-257.8	-49.07	-6.61	0.9784
	HW15	Xianquan	9.00 E-07	6.5	0.64	0.62	7.5	92.5	-23.7	-36.7	-708.9	-258.1	-48.66	-6.35	0.9867
Middle	HW01	Lijun	8.36 E-07	475.6	0.60	0.60	7.3	92.7	-14.1	-34.8	-821.7	-220.5	-61.88	-8.32	0.9790
Middle	HW04	Hongri	8.46 E-07	218.6	0.60	0.60	7.3	92.7	-18.2	-35.7	-739.1	-281.8	-57.45	-7.90	0.9822
	HW09	Fengquan	8.33 E-07	51.7	0.60	0.60	7.2	92.8	-13.3	-33.2	-771.7	-256.6	-57.11	-7.86	0.9798

^a Rc/Ra is the air-corrected He isotope ratio = [(R/Ra)X-1]/(X-1); where X is the air-normalized respective ratio: X = $({}^4\text{He}/{}^{20}\text{Ne})_{\text{measured}}/({}^4\text{He}/{}^{20}\text{Ne})_{\text{air}}$ (Duchkov et al., 2010).

^b The portion of mantle helium (X_m) and crustal helium ($1-X_m$) can be calculated with the following formula: $R_c/\text{Ra} = 8X_m + 0.02(1 - X_m)$, by assuming ${}^3\text{He}/{}^4\text{He}$ values of MORB and crust as 8 Ra and 0.02 Ra (Sano and Wakita, 1985; Karakuş, 2015).

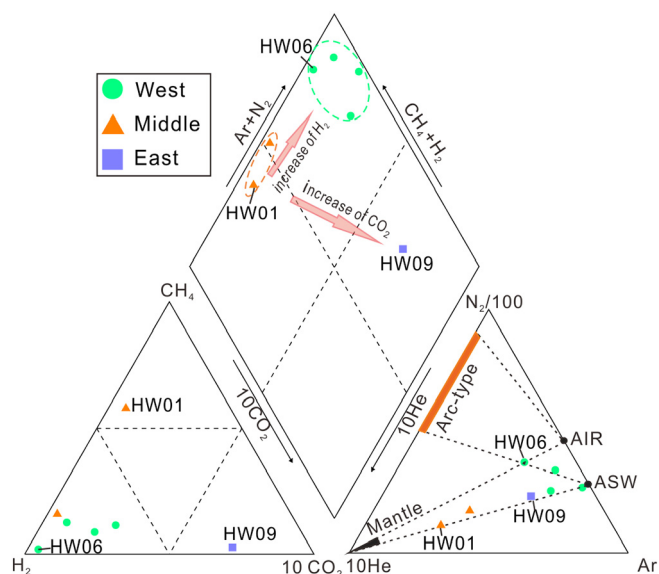


Fig. 2. Trilinear diagram for distinguishing gas types and evolutionary pathways in the study area. This diagram consists of three parts: a reactive gas triangle for showing the relative percentages of H₂, CH₄ and CO₂, a nonreactive-gas triangle for showing the relative percentages of N₂, He and Ar, and a central diamond-shaped field (quadrilateral field) for showing the overall chemical characteristics of the gas. The nonreactive-gas triangle is modified from Zimmer et al. (2004) with the following end-members: air (AIR), air-saturated water (ASW), a mantle-derived component and volcanic arcs (Arc-type). High N₂/He in arcs (800–8000) vs. values of 10–150 in the mantle-derived gas has been attributed to the addition of N from marine sediments (Zimmer et al., 2004; Fiebig et al., 2004; Fischer et al., 2002; Gigganbach, 1992). It should be noted that the CO₂ and He concentrations are both multiplied by 10, and that of N₂ is divided by 100 to present the differences in the gases in the study area clearly.

4.2. Isotope composition of water and gas discharge

In the plot of δD versus $\delta^{18}\text{O}$, the geothermal waters in the study area plot on the LMWL, indicating a dominant meteoric origin, and they exhibit wide ranges of δD values (-61.9 to -45.8‰) and $\delta^{18}\text{O}$ values (-8.3 to -6.1‰) in an increasing trend from the central to the western and eastern parts (Fig. 3A). Combined with the plot of $\delta^{18}\text{O}$ versus TDS (Fig. 3B), the trend indicates that hot water mixes with increased proportions of shallow groundwater from the central (HW01) to the western and eastern parts.

The ${}^3\text{He}/{}^4\text{He}$ ratios are relatively constant with a range of 0.55 Ra to 0.65 Ra (Table 2). And ${}^4\text{He}/{}^{20}\text{Ne}$ ratios (6.5–475.6) for geothermal waters are 20–1496 times higher than those of the air ratio (0.318) and

air-saturated water (~0.26 at 10 °C), which indicates that the helium isotope composition was not strongly affected by atmospheric helium (Tardani et al., 2016; Karakuş, 2015). For most gas samples, the atmospheric helium contribution to gas samples is below 1% except HW11 (1%) and HW15 (5%) (Fig. S3 of the Supplementary material). In order to assess the proportions of mantle-derived and crustal helium, all measured ${}^3\text{He}/{}^4\text{He}$ ratios were corrected for possible air contamination by assuming that all measured Ne was of atmospheric origin (Craig et al., 1978; Karakuş, 2015). The air correction results in only a minor adjustment (< 0.02) to the measured R/Ra. The air-corrected Rc/Ra ratios range from 0.54 to 0.65, and indicate a dominant crustal source (about 92–93%) for helium, with 6–8% mantle helium contributions in the samples (Table 2).

The δD values for H₂ range from -822 to -709‰ and exhibit a trend similar to those for water isotopes. By contrast, the δD values for CH₄ show the opposite tendency. The CH₄ in the central part, especially in HW01, is the richest in deuterium (-221‰) compared with those of the western and eastern parts (-428 to -250‰). The trends in $\delta^{13}\text{C}_{\text{CO}_2}$ and $\delta^{13}\text{C}-\text{CH}_4$ are in a decreasing order of east > central > west.

It should be noted that in the extreme cases for each part, the gas from HW06 in the western part with the highest H₂ content (12.5 vol%) and the lowest content of CH₄ (0.3 vol%) is the most depleted in the deuterium of the CH₄ (-428‰). In the central part, HW01 reflects the original information from depth to the greatest extent due to the least mixing of shallow fluids as previously mentioned, and it exhibits the lowest H₂ concentration (2.4 vol%) and δD value (-822‰), which is the most deuterium-depleted H₂ found in nature, except for the value of -836‰ in Kansas (Coveney et al., 1987). The gas from HW09 in the eastern part is characterized by a high CO₂ concentration (1.89 vol%), CO₂/CH₄ ratio (2.6), $\delta^{13}\text{C}_{\text{CO}_2}$ (-13.3‰) and $\delta^{13}\text{C}-\text{CH}_4$ (-33.2‰).

5. Discussion

5.1. Origin of the gases

5.1.1. Hydrogen gas origin

The abnormally high H₂ level (2.4–12.5 vol%) in the study area is unusual in sedimentary-dominated, low continental geothermal systems and in a dramatic contrast to the gases of other geothermal systems along the eastern coastal area and the Tanlu fault zone dominated by N₂, CO₂ or CH₄, with trace H₂ (< 0.5%) (Fig. S1). An effective way to fingerprint H₂ is to use its isotope patterns. Here, previous studies on the hydrogen isotopes of H₂ produced from different mechanisms in various geological environmental and experimental conditions have been systematically reviewed to restrict the dominant origin of H₂ (Fig. 4). Specifically, δD values of mantle materials (e.g. OH-bearing minerals and water extracted from basaltic rocks) are -80 to -50‰

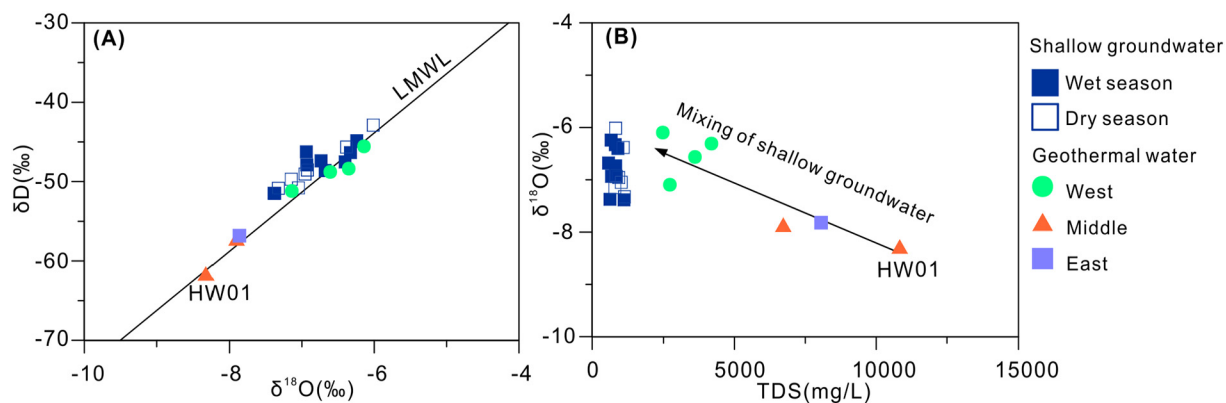


Fig. 3. (A) Plot of δD versus $\delta^{18}\text{O}$ for the waters in the Jimo Basin; local meteoric water line (LMWL) based on the isotope composition data for the precipitation over eastern China (Liu et al., 2009). The shallow groundwater data is from Table S1. (B) Plot of $\delta^{18}\text{O}$ versus TDS showing the mixing of shallow groundwater.

(Kyser, 1986; Sano et al., 1993). The hydrogen isotopes (δD) and the actual isotope fractionation factors for H_2O and H_2 ($\alpha_{\text{H}_2\text{O}-\text{H}_2}$) in geothermal systems are related to their geological conditions; the wide ranges of the δD (−836 to −372‰) and $\alpha_{\text{H}_2\text{O}-\text{H}_2}$ (1.6 to 5.5) values are dependent on the temperature of the serpentinite-hosted hydrothermal system (Vacquand et al., 2018; Neal and Stanger, 1983; Suda et al., 2014; Proskurowski et al., 2006; Taran et al., 2010; Abrajano et al., 1988; Coveney et al., 1987; Maruyama, 2014); for the deep seafloor hosted by basalt and sediments, the δD values range from −635 to −328‰, and relatively low $\alpha_{\text{H}_2\text{O}-\text{H}_2}$ values of 1.5 to 2.7 are observed (Suda et al., 2014; Proskurowski et al., 2006); δD values of −675 to −110‰ and $\alpha_{\text{H}_2\text{O}-\text{H}_2}$ values of 1.1 to 2.5 are reported for continental volcanic gases (Kiyosu, 1983; Taran et al., 1992; Mizutani, 1983; Arnason, 1977; Arnason and Sigurgeirsson, 1968; Lyon and Hulston, 1984; Gunter and Musgrave, 1971; Neal and Stanger, 1983); and δD values of −791 to −242‰ and $\alpha_{\text{H}_2\text{O}-\text{H}_2}$ values of 1.2 to 4.4 occur in fault zones (Sugisaki et al., 1983; Shangguan et al., 2000; Shangguan and Huo, 2002; Kita et al., 1980). Other mechanisms have been reported in limited hydrogen isotope studies, such as gas mediated by microbial sulfate reduction being characterized by δD values of −689 to −646‰ and $\alpha_{\text{H}_2\text{O}-\text{H}_2}$ values of 2.8 to 3.2 (Proskurowski et al., 2006; Krichevsky et al., 1961); −814 to −763‰ for the δD values and 4.4 to 5.1 for the $\alpha_{\text{H}_2\text{O}-\text{H}_2}$ values have been observed in marine experiments (Krichevsky et al., 1961); corrosion-induced H_2 with δD and $\alpha_{\text{H}_2\text{O}-\text{H}_2}$ values of −277‰ and 1.4, respectively, have been determined for a geothermal well in a northern German basin (Feldbusch et al., 2018), and values of −600‰ and 2.4, respectively, were found for a well water in New Zealand (Lyon and Hulston, 1984); and the radiolytic reactions in H_2 that take place in several Precambrian shields are characterized by a constant $\alpha_{\text{H}_2\text{O}-\text{H}_2}$ value of 2.05 ± 0.07 (Lin et al., 2005). Besides, a large accumulation of H_2 with a δD value of −702‰, has been found for a well drilled in Proterozoic sedimentary formations, interlayered with dolerite sills of Triassic age in Mali, which is most likely issued from the deep cratonic basement and accumulated at shallow depth. But the specific generation mechanism has not been proposed (Prinzhofen et al., 2018). It should be noted that this data compilation is a preliminary tool to identify the dominant origin of H_2 . Because the limited δD analysis for H_2 in the published literature and overlap in the δD of H_2 with different origins add the uncertainty and reduce the sensitivity of restricting the dominant origin of H_2 , which is also a limit of other framework plots (Etiope and Sherwood-Lollar, 2013). Besides, the genetic signature covered by post-genetic processes (e.g. mixing, oxidizing and diffusion) (Pernaton et al., 1996; Prinzhofen and Pernaton, 1997; Krooss and Leythaeuser, 1988, 1992; Krooss et al., 1988, 1992; Krooss and Schaefer, 1987) is also a challenge for the use of hydrogen isotopes of H_2 directly to identify the hydrogen origin.

The hydrogen from various natural environments generally has higher δD values and lower isotope fractionation with H_2O than those

from the Jimo hot spring (Fig. 4). Moreover, because the isotope exchange rates between H_2 and H_2O is lower than the cooling rate of water, the predicted temperatures are generally higher than the measured values, and most gas samples plot above the equilibrium line (Fig. 5A) (Suda et al., 2014; Proskurowski et al., 2006). However, the gases from the study area plot below the equilibrium line, which indicates that the hydrogen isotope disequilibrium between H_2O and H_2 cannot be attributed to a common rapid cooling process. In addition, as the $\text{CH}_4-\text{H}_2-\text{H}_2\text{O}$ hydrogen isotope schematic (Fig. 5B) shows, the gas from HW01 in the study area greatly deviates from the full equilibrium line observed in $\text{H}_2-\text{CH}_4-\text{H}_2\text{O}$ and is beyond the range of previous studies. The isotope exchange between H_2 and H_2O is more rapid than the CH_4 and H_2O exchanges (Wang et al., 2018; Kiyosu, 1983; Suda et al., 2014; Proskurowski et al., 2006; Arnason, 1977). However, for HW01, which reflects the original information from depth to the greatest extent, a near equilibrium between CH_4 and H_2O is achieved at 95 °C based on the isotope equilibrium equation (Horibe and Craig, 1995), which is close to the measured wellhead temperature (89.5 °C). By contrast, the isotope exchange between H_2 and H_2O is far from equilibrium with an abnormally low calculated temperature (< 0 °C) (Fig. 5B, Table S2). Therefore, this discordance may indicate a different origin for H_2 with CH_4 .

A few gas samples that plot below the equilibrium line and extremely deuterium-depleted H_2 have also been found at specific locations, such as in the Tengchong (−791‰) and Yamasaki regions (−770 to −470‰) in relation to fault activity (Shangguan and Huo, 2002; Kita et al., 1980), microbial reactions in marine experiments (Krichevsky et al., 1961), and Kansas (−836 to −740‰), as caused by water reduction and Fe^{2+} oxidation (e.g., serpentinization) (Coveney et al., 1987). Combined with the geological conditions and geochemical characteristics of geothermal fluids, the following three mechanisms potentially causing the depleted hydrogen isotope composition have been discussed: (1) water reduction and ferrous iron oxidation; (2) the mechanism related to an active fault with significant isotope kinetic fractionation; and (3) microbial origin.

5.1.1.1. Water reduction and ferrous iron oxidation. H_2 can be produced by hydrolyzing mafic or ultramafic rock through the water reduction and oxidation of metals (Fe^{II} , Mn^{II} , Ni^{II} , etc.), with Fe^{II} in particular being by far the most abundant electron donor in the ultrabasic-basic rocks (Vacquand et al., 2018). During these reactions, Fe^{II} is oxidized to Fe^{III} , such as magnetite (Fe_2O_3) or Fe^{III} -bearing serpentine, and water reduction generates H_2 .

Although the geothermal reservoir is dominated by sandstone, basalt and schönfelsite from the Bamudi Formation (K_1qb) in the study area is located approximately 2 km northwest of the geothermal system (Fig. 1B). Jimo basaltic samples are commonly subaphyrptic to weakly porphyritic with phenocrysts consisting of pyroxene and minor olivine

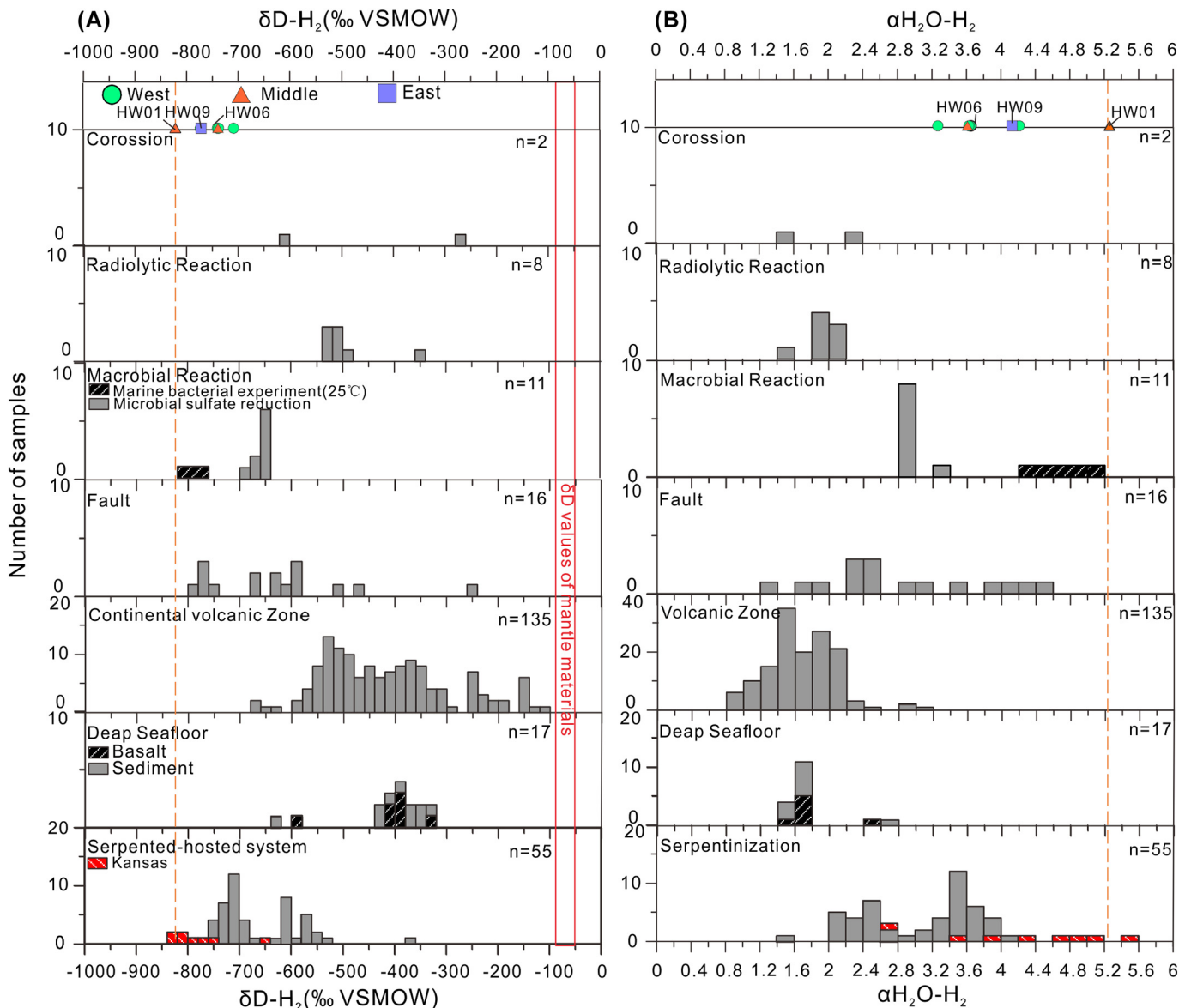
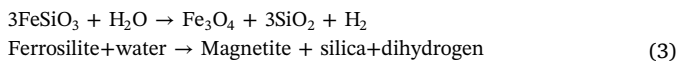
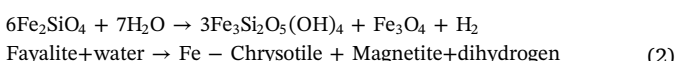
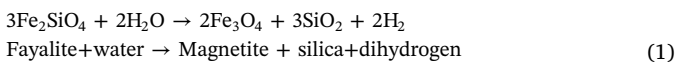


Fig. 4. (A) Summary of the δD -H₂ values and (B) αH_2O -H₂ datasets from different systems: hydrogen isotope of mantle materials (Kysar, 1986; Sano et al., 1993); serpentinite-hosted hydrothermal systems (Vacquand et al., 2018; Neal and Stanger, 1983; Suda et al., 2014; Proskurowski et al., 2006; Taran et al., 2010; Abrajano et al., 1988; Coveney et al., 1987); deep seafloor hydrothermal systems hosted by basalt and sediments (Suda et al., 2014; Proskurowski et al., 2006); continental volcanic zones (Kiyosu, 1983; Taran et al., 1992; Mizutani, 1983; Arnason, 1977; Arnason and Sigurgeirsson, 1968; Lyon and Hulston, 1984; Gunter and Musgrave, 1971; Neal and Stanger, 1983); fault zones (Sugisaki et al., 1983; Shangguan et al., 2000; Shangguan and Huo, 2002; Kita et al., 1980); H₂ produced by other mechanisms with limited studies: microbial reaction (Proskurowski et al., 2006; Krichevsky et al., 1961); corrosion (Feldbusch et al., 2018; Lyon and Hulston, 1984); and radiolytic reactions (Lin et al., 2005). The red solid zone and orange dashed line represent the isotope characteristics of H₂ from mantle materials and HW01, respectively, and n represents the total number of samples. (For interpretation of the references to color in this figure legend, the reader is referred to the web version of this article.)

with grain sizes of 2–4 mm. The matrix is primarily composed of fine-grained clinopyroxene and plagioclase and a few opaque oxides (Fan et al., 2001; Zhang and Sun, 2002). Therefore, Fe^{II}-rich pyroxene and olivine minerals may provide Fe²⁺ for the following olivine hydration (Eqs. (1), (2)) and ferrosilite hydrolysis (Eq. (3)) to produce H₂ (Oze and Sharma, 2005):



Because the average estimated temperature of the geothermal reservoir is ~140 °C (below 150 °C) (Table S3), the formation of Fe-chrysotile (Eq. (2)) is favorable for olivine hydration (Oze and Sharma, 2005). Combined with the geologic settings and hydrological flow system, the study area is a palm-like basin that is surrounded by mountains on three sides (Fig. 1C), and it is recharged by infiltrated meteoric water from the surrounding mountains (Hao et al., 2019; Wan and Zhang, 1987). The NW extensional Dongkuang-Shiubo fault is a water-conducting fault. Therefore, it is likely that H₂ is generated by water reduction and Fe²⁺ oxidation from basalt in the Bamudi Formation of the Qingshan Group located 2 km northwest of the

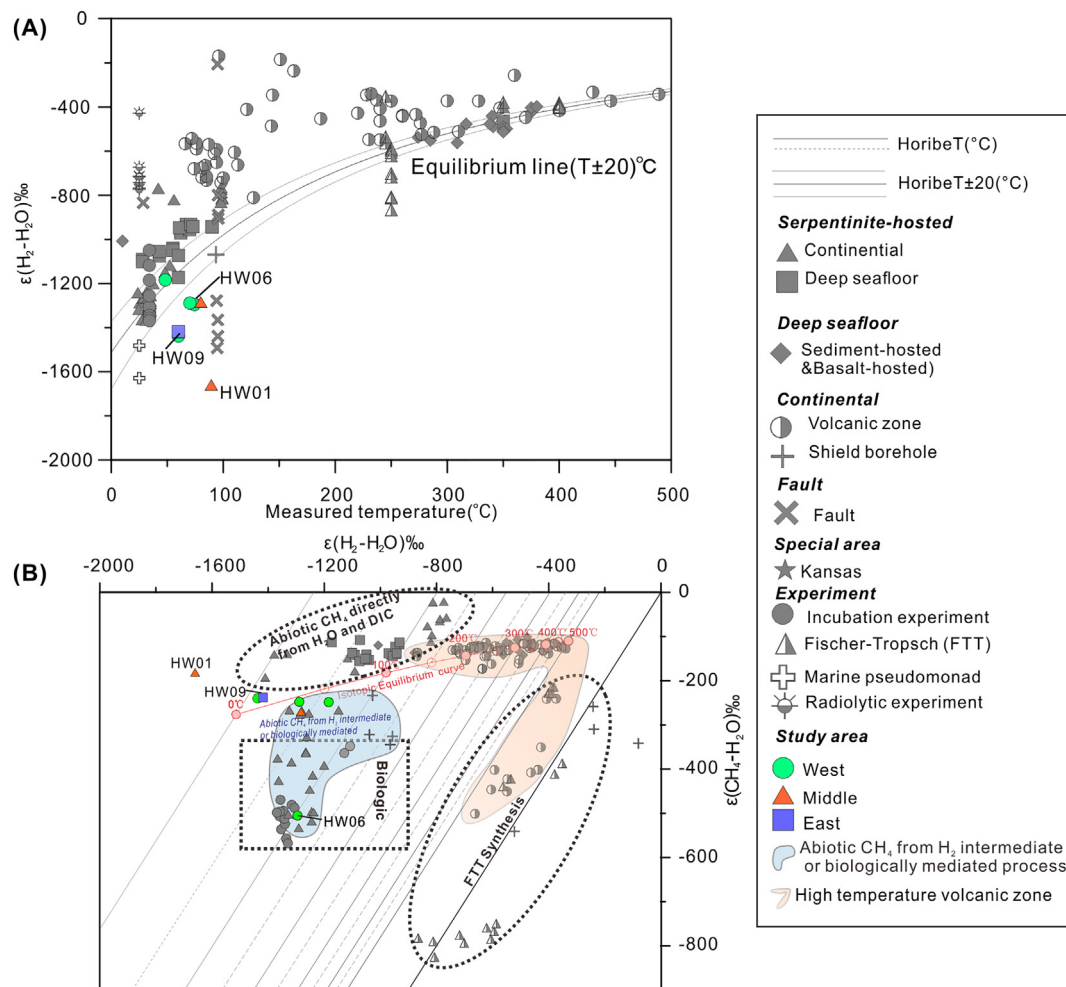


Fig. 5. Relationships between (A) measured fractionation and thermodynamically predicated equilibrium fractionation at a given temperature for $\text{H}_2\text{-H}_2\text{O}$, (B) $\varepsilon(\text{H}_2\text{-H}_2\text{Oaq})$ and $\varepsilon(\text{CH}_4\text{-H}_2\text{Oaq})$ of the Jimo gas samples compared with those of the gases documented in natural environments adapted from (Suda et al., 2014) as follows: continental serpentinite-hosted systems (Suda et al., 2014; Proskurowski et al., 2006; Neal and Stanger, 1983; Vacquand et al., 2018), deep seafloor serpentinite-hosted systems (Suda et al., 2014; Proskurowski et al., 2006), deep seafloor hydrothermal systems hosted by basalt and sediments (Proskurowski et al., 2006; Horibe and Craig, 1995), continental volcanic zones (Kiyosu, 1983; Taran et al., 1992; Arnason, 1977; Arnason and Sigurgeirsson, 1968; Gunter and Musgrave, 1971; Neal and Stanger, 1983; Lyon and Hulston, 1984), shield boreholes (Sherwood-Lollar et al., 1993), fault zones (Sugisaki et al., 1983; Shangguan et al., 2000; Shangguan and Huo, 2002) and Kansas (Coveney et al., 1987). The experimental conditions for CH_4/CO_2 formation included microbial methanogens (Balabane et al., 1987), abiogenic methane production via FTT synthesis (Fu et al., 2007; Taran et al., 2010; McCollom et al., 2010), H_2 formation in a marine pseudomonad (Krichevsky et al., 1961) and radiolytic H_2 reactions (Lin et al., 2005; Blair et al., 2007). The $\text{CH}_4\text{-H}_2\text{-H}_2\text{O}$ hydrogen isotope systematics are modified from Suda et al. (2014). The ε value is calculated according to the following equations: $\varepsilon = 1000\ln\alpha$, with $\alpha(\text{H}_2\text{O}_{\text{aq}}\text{-H}_2) = 1.0473 + 201,036/T^2 + 2.060 \times 10^9/T^4 + 0.180 \times 10^{15}/T^6$ and $\alpha(\text{H}_2\text{O}_{\text{aq}}\text{-CH}_4) = 1.0997 + 8456/T^2 + 0.9611 \times 10^9/T^4 - 27.82 \times 10^{12}/T^6$ (Suda et al., 2014; Horibe and Craig, 1995).

geothermal system and then it migrates into the sandstone via the dominant NW extensional fault. This inference is also reasonable from the perspective of the hydrogen isotope ratio of H_2 . The 8D values for H_2 in the study area fall within the range of those produced by water reduction and Fe^{2+} oxidation from a serpentinite-hosted hydrothermal system with 8D values from -836 to -372‰ (Fig. 4). 8D- H_2 values are comparable to the lowest values recorded in nature (Coveney et al., 1987) of -740 to -836‰ in Kansas which is likely caused by water reduction and Fe^{2+} oxidization at approximately 10°C , especially for HW01 (-822‰). Low 8D values generally represent the generation of H_2 at relatively low temperatures (Vacquand et al., 2018; Sherwood-Lollar et al., 1988; Neal and Stanger, 1983). The temperature calculated based on the isotope equilibration of H_2 and H_2O from HW01 is lower than 0°C (Fig. 5B), which may reflect the generation of H_2 at a low near-ambient temperature. The slight deviations in the near-ambient temperatures (generally $>0^{\circ}\text{C}$) may be attributed to the uncertainty of the water isotope composition that are exchanged with H_2 (Coveney et al., 1987) or a diffusional migration effect (Sherwood-Lollar et al.,

1993; Etiopic and Sherwood-Lollar, 2013; Pernaton et al., 1996; Prinzhofner and Pernaton, 1997). In fact, a calculation of the isotope temperature should be established between the H_2 and the meteoric water at the recharge time rather than the geothermal water of HW01. According to the previous water isotope and radio carbon (^{14}C) age (Hao et al., 2019), the geothermal system is recharged by meteoric water formed during the Pleistocene glacial period ($>10,000$ years), which is dominated by a colder climate and the temperature is $7\text{--}13^{\circ}\text{C}$ lower than the present-day temperature (Huang and Sun, 2007; Zhang et al., 1999). Accordingly, the 8D value for paleo-meteoric water should be $39\text{--}73\text{‰}$ lower than modern meteoric water (Clark and Fritz, 1997). As the infiltrated paleo-meteoric water has evolved into HW01 geothermal water, the shallow groundwater recharged by present meteoric water with higher 8D- H_2O values has been mixed in (Fig. 3). Therefore, the isotope temperature based on the H_2 and geothermal water of HW01 is slightly lower. Diffusion can also result in deuterium depletion in the migrating gas by preferentially removing the isotopically light species both in an aqueous or a gaseous phase. And the isotope

fractionation in an aqueous phase may be relatively smaller than that in a gaseous phase, but still significant (Sherwood-Lollar et al., 1988, 1993; Pernaton et al., 1996; Prinzhofner and Pernaton, 1997; Krooss and Leythaeuser, 1988, 1992; Krooss et al., 1988, 1992; Krooss and Schaefer, 1987). The amounts and rates of H₂ production are related to the rock type, the proportion of Fe^{II} converted to Fe^{III}, the water/rock ratio, temperature, surface passivation and the minor phases (e.g., spinels) (McCollom and Bach, 2009; McCollom et al., 2016; Wetzel and Shock, 2000; Klein et al., 2009, 2013, 2014, 2015a, 2015b; Frost and Beard, 2007; Mayhew et al., 2013). Additionally, the water-basalt reaction generates much lower H₂ concentrations (generally 0.05–1.7 mmol/kg) than the serpentinization of ultramafic rocks (e.g., 12–16 mmol/kg) (McCollom and Bach, 2009; Keir, 2010; Wetzel and Shock, 2000; Wang et al., 2018). In the deep environment, at high pressure and temperature conditions, the solubility of H₂ far exceeds the production capacity; for example, the solubility reaches up to 233 mmol/L at 300 atm and 100 °C, which causes H₂ to enter a dissolved state without a free gas phase. However, during the initial production at near-surface conditions (e.g., 0–25 °C and 101 kPa), the solubility of H₂ is 0.8–0.9 mmol/kg. It can thus be inferred that if the H₂ production is > 0.8–0.9 mmol/kg, such as 1–1.7 mmol/kg, it is possible for H₂ to migrate as a free gas. Since the basalts in the study area have well developed fumarole-amygduoidal structures and fractures (Fan et al., 2001) and they have been cut by the dominant NW extensional Dongkuang-Shuibo fault (Fig. 1C), the production of H₂ > 0.8–0.9 mmol/kg is possible. In conclusion, the diffusional effect cannot be ruled out. And the diffusion form (in an aqueous phase or a gaseous phase) and isotope fractionation caused by diffusion effect is required to quantified by further mathematical modelling and laboratory experiments.

5.1.1.2. Role of an active fault. Gases with high H₂ or CO₂ levels also occur in active faults (Kita et al., 1980; Sugisaki et al., 1983; Shangguan et al., 2000; Shangguan and Huo, 2002). The types of gases are dependent on the rock types through which the fault cuts; specifically, CO₂ and H₂ tend to be found in sedimentary and igneous rocks, respectively. The gas concentration fluctuates considerably and is closely related to the fault activity. In general, the H₂ concentrations from active faults associated with historical earthquakes can be up to several percent, whereas in most conditions, 100 ppm is linked to Quaternary faults without historical earthquakes (Sugisaki et al., 1983).

In the study area, the dominant NE- and NW-trending faults have become stable since the Holocene and have no modern seismicity records (Luan and Zhang, 2001). In addition, if the gas production is related to the fault zone, a higher CO₂ concentration should be observed instead of the H₂ since sandstone is the dominant rock of the geothermal reservoir crossed by both NE- and NW-trending faults (Fig. 1B). The low concentration of CO₂ (0.04 vol%) indicates that gas production is not primarily controlled by the faults. Therefore, the high H₂ level in the study area cannot be generated by this mechanism (Kita et al., 1980; Sugisaki et al., 1983).

Outgassing from the mantle may also be difficult to accommodate because of the high concentrations (2.4–12.5 vol%) and low isotope ratios of H₂ (−822 to −709‰) in the study area. The R/Ra ratios in the study area range from 0.55 to 0.65 (Table 2), indicating a primary crustal origin with 6–8% mantle contributions for helium. R/Ra ratios in the study area are consistent with those of other geothermal systems along the Tanlu fault zone and eastern coastal areas (0.32–0.76) (Minissale et al., 2008; Liu et al., 2001; Shangguan et al., 1998), which have similar tectonic properties (Fig. S3). However, the trace H₂ levels (< 0.5%) in these geothermal systems preclude a mantle-dominated origin for the high H₂ level in the study area. In addition, mantle materials (e.g. OH-bearing minerals and water extracted from basaltic rocks) are rich in deuterium and with δD values of −80 to −50‰. And δD values of H₂ (−822 to −709‰) in the study area are too low to agree with a significant mixture of mantle-derived H₂ (Coveney et al.,

1987; Kita et al., 1980; Sano et al., 1993).

5.1.1.3. Microbial factor. The hydrogen concentration produced by the bacterially mediated fermentation of organic matter depends significantly on the temperature (Hoehler et al., 1998; Bradley and Summons, 2010; Kashefi and Lovley, 2003). The average temperature of the geothermal reservoir is estimated to be up to 137 ± 13 °C (Table S3) and is above the highest temperature at which microbes can survive (121 °C) (Kashefi and Lovley, 2003), which will prevent the bacterial activity that produces H₂. In addition, the increasing trend in the δD values with the mixing of biogenic H₂ in the shallow aquifers (Fig. 9, as discussed in 5.2) indicates that the H₂ produced by bacteria in the study area should be rich in deuterium (δD > −774‰ to −709‰). Therefore, the H₂ with depleted deuterium cannot be attributed to a microbial origin.

In conclusion, the H₂ from the deep reservoir is most likely generated at 2 km northwest of the geothermal system by the reduction of water and the oxidation of Fe^{II}-bearing pyroxene and olivine (Serpentinization of Pyroxene and Olivine) in basalts at low temperatures, and it then migrated into the sandstone via the NW-trending fault.

5.1.2. Methane gas origin

Methane can be divided into biotic and abiotic methane according to the direct involvement of organic matter (Etiope and Sherwood-Lollar, 2013). Biotic methane includes microbial CH₄ formed at low temperatures of generally < 100 °C (Fiebig et al., 2004; Schoell, 1988; Whiticar et al., 1986) and thermogenic CH₄ produced at temperatures higher than 100 °C (Schoell, 1988; Des Marais et al., 1981). Abiotic methane without the direct involvement of organic matter is generally related to high-temperature magmatic processes or gas-water-rock reactions at low temperatures (Etiope and Sherwood-Lollar, 2013; Suda et al., 2014; Proskurowski et al., 2006). The differences in the carbon and hydrogen isotope composition between biotic and abiotic methane are useful tools for identifying the methane formation mechanisms (Etiope and Sherwood-Lollar, 2013).

The plot of δ¹³C-CO₂ versus δ¹³C-CH₄ (Fig. 6A) suggests predominantly thermogenic origins for the CH₄ and CO₂, which is also supported by the sandstone-hosted geothermal reservoir with abundant organic materials. However, according to the relationship between the hydrogen and carbon isotopes of CH₄ (Fig. 6B), the HW01 sample falls within the thermogenic zone and the boundary of the abiotic zone, which makes the methane origin ambiguous. When considering deep-seated H₂ with an abiotic origin that was produced in basalt, the possibility of abiotic CH₄ produced by the corresponding reduction of CO₂ via Fischer-Tropsch reactions (Vacquand et al., 2018; Suda et al., 2014; McCollom and Bach, 2009) has been considered and ruled out for the following reasons: (1) The significantly abiotic CH₄ produced by the above reactions needs strongly reducing conditions and abundant metal catalysts (Fe, Ni, Cr and Ru). It generally takes place in ultramafic-hosted hydrothermal systems and is characterized by hyperalkaline fluids with pH = 10–12 (i.e., Ca-OH type waters), and extreme hydrogen enrichment, but they have low occurrences in mafic-hosted systems (Vacquand et al., 2018; McCollom and Bach, 2009; Wang et al., 2018; Keir, 2010). In the study area, the basalt and geochemical signatures of HW01 (H₂/CH₄ < 1, nearly neutral water) disagree strikingly with an abiotic CH₄ origin. (2) The CH₄-H₂-H₂O disequilibrium conditions reflect different origins for the H₂ and CH₄, which imposes constraints on the migration of CH₄ with H₂ from the basalt rocks to the sandstone reservoir.

Above all, the principal source of CH₄ and CO₂ at depth is the thermal decomposition of organic materials in the sandstone of the Laiyang Group.

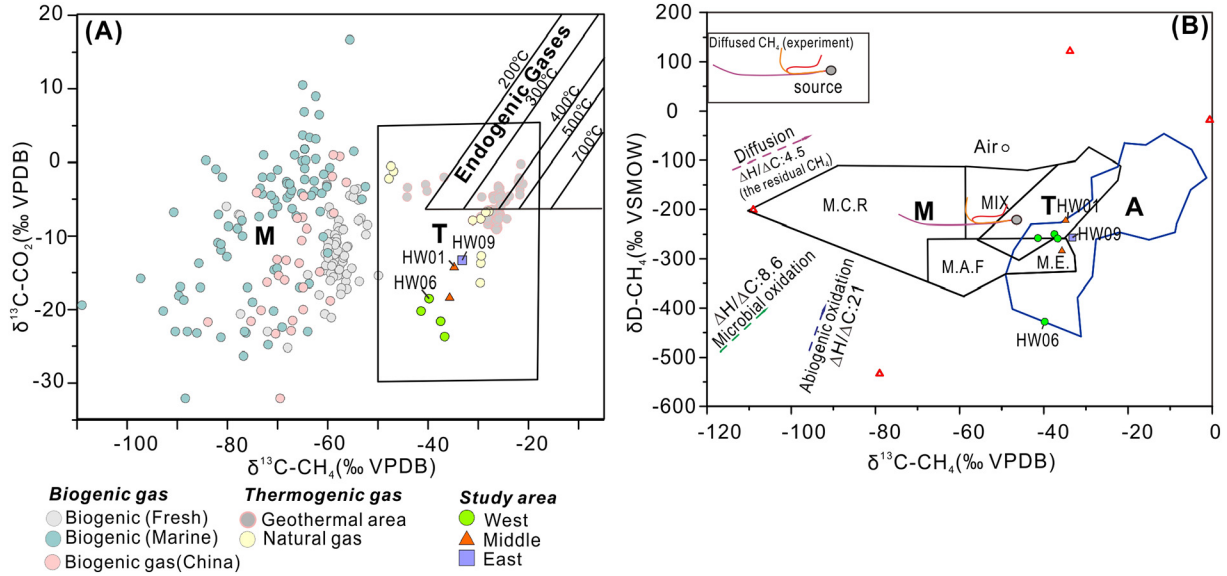


Fig. 6. (A) $\delta^{13}\text{C}-\text{CO}_2$ versus $\delta^{13}\text{C}-\text{CH}_4$; the gas samples in the study area are compared to the biogenic gases (M) documented in a fresh environment and in a marine environment (Whiticar et al., 1986), thermogenic gas from hydrothermal systems (Kotarba and Nagao, 2015; Lowenstern et al., 2012; Tian et al., 2018) and natural gas (Kotarba et al., 2014). The compositional fields of thermogenic (T) and endogenic gases are modified from Kotarba et al. (2014). (B) $\delta\text{D}-\text{CH}_4$ versus $\delta^{13}\text{C}-\text{CH}_4$, modified from Etiope and Sherwood-Lollar (2013) and Etiope et al. (2011a, 2011b). T: thermogenic CH_4 ; M: microbial CH_4 ; M.C.R.: microbial CH_4 from carbonate reduction; M.A.F.: microbial CH_4 from acetate fermentation; M.E.: microbial CH_4 from an evaporitic environment; and A: abiotic CH_4 . The red open triangles represent the lowest and highest $\delta^{13}\text{C}-\text{CH}_4$ and $\delta^{13}\text{D}-\text{CH}_4$ values found in natural gas systems (Etiope et al., 2011a, 2011b). The fractionation slopes of diffusion, microbial or abiogenic oxidation for the residual gas is from Etiope and Sherwood-Lollar (2013). Isotope results of the diffused methane with different fractionation are based on various diffusion experiments of a starting material in the thermogenic field through shales (Pernaton et al., 1996).

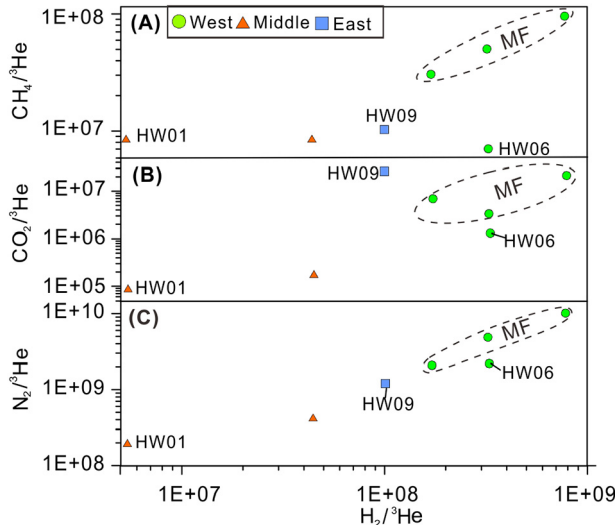


Fig. 7. Plots of $\text{CH}_4/{}^3\text{He}$ vs. $\text{H}_2/{}^3\text{He}$, $\text{CO}_2/{}^3\text{He}$ vs. $\text{H}_2/{}^3\text{He}$, and $\text{N}_2/{}^3\text{He}$ vs. $\text{H}_2/{}^3\text{He}$. MF: mixing of gases from shallow fresh environments.

5.2. Evolution of the gases in the shallow aquifer

5.2.1. Evolutionary path I

As a strongly reducing gas, hydrogen is usually consumed along its flow path in a geothermal system (Shangguan and Huo, 2002). However, in the study area, the hydrogen concentration increases along the flow path from the central part (2.4%) to the eastern (7.3%) and western (5.6% to 12.5%) parts, which may indicate that considerable portions of the H_2 from a shallow environment have been mixed in along the flow path. Hydrogen isotopes for H_2 are used to reveal this evolution. In contrast to HW01, the hydrogen isotope compositions of H_2 seem to be close to equilibrium with H_2O and CH_4 from the central to the eastern and western parts, except for that for HW06 (Fig. 5A, B).

The calculated $\text{H}_2\text{O}-\text{H}_2$ and $\text{CH}_4-\text{H}_2\text{O}$ equilibrium temperatures (except HW01) with a range of 10 to 52 °C and below 0 to 31 °C, respectively, are approximately 40 °C lower than the average measured temperatures at the wellhead (Table S2). Therefore, equilibrium is not the primary reason for the changes in the hydrogen isotope ratios. Instead, the gas samples gradually approaching the biogenic zone (Fig. 5B) indicate the mixing of biologic gases (CH_4 and H_2) formed at low temperatures. Combined with the local environment, the microbial H_2 is most likely from the overlaid organic-rich unconsolidated Quaternary sediments (e.g., lagoon clays and lacustrine silty sediments) (Liu et al., 2009), which could be regarded as the organic-rich aquitard sediments (low-permeability sediments stratigraphically adjacent to higher-permeability aquifer sediments). These aquitard sediments have high fermentative capacity of sedimentary organic matter and insignificant consumption activity (e.g. sulfate-reducing microorganisms and methanogenic activity). Therefore, the production rate of H_2 exceeds the consumption rate, resulting in a net accumulation of H_2 (McMahon and Chapelle, 1991). Then the concentration gradient drives the microbial H_2 from the aquitards to geothermal fluids, causing the increase of H_2 concentration.

The addition of microbial H_2 is also rational from the perspective of other associated gas signatures (e.g., CH_4 and CO_2). The generally similar increasing trends in $\text{CH}_4/{}^3\text{He}$ (except HW06), $\text{CO}_2/{}^3\text{He}$ (except HW09) and $\text{H}_2/{}^3\text{He}$ from the central part (2.4%) to the eastern (7.3%) and western (5.6% to 12.5%) parts indicate that the additions of H_2 , CH_4 , and CO_2 are coupled (Fig. 7).

The decrease in the $\delta^{13}\text{C}$ value and the increased $\text{CO}_2/{}^3\text{He}$ from the central to the western part (Fig. 8A) reflect the mixing of organic carbon from sediments with high $\text{CO}_2/{}^3\text{He}$ (1×10^{13}) and low ${}^{13}\text{C}$ values ($-30 \pm 10\text{‰}$). The addition of microbial CH_4 from the central to the western part can be identified by the samples (except HW06) that gradually approach the microbial zone (Fig. 6B). Although post-genetic processes might change the carbon and hydrogen isotope compositions of CH_4 after its formation and during migration (Etiope and Sherwood-Lollar, 2013; Pernaton et al., 1996; Prinzhofner and Pernaton, 1997), the increase of $\text{CH}_4/{}^3\text{He}$ ratio and synchronous decrease of $\delta\text{D}_{\text{CH}_4}$ and

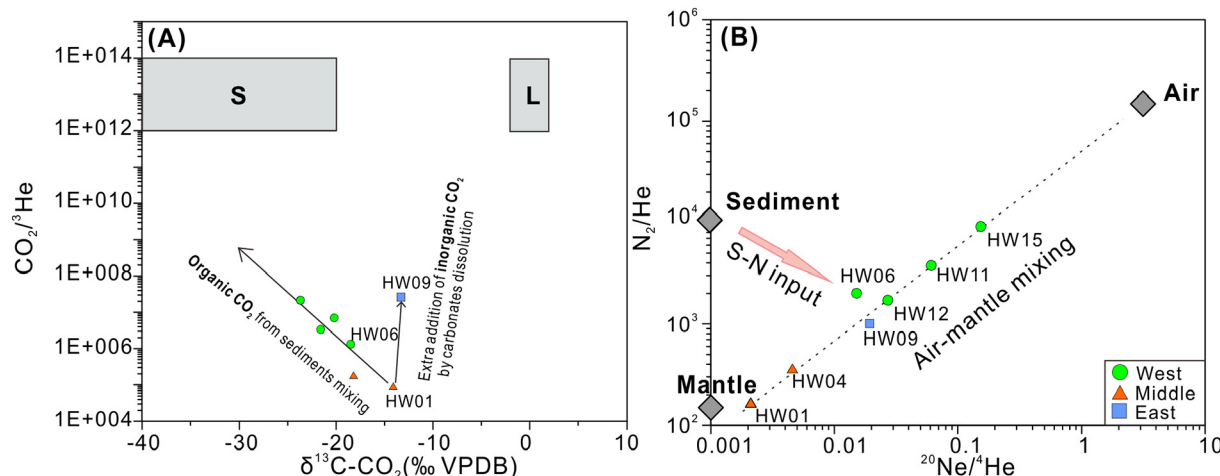
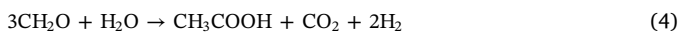


Fig. 8. (A) $\text{CO}_2/\text{He}^{3\text{He}}$ vs. $\delta^{13}\text{C}-\text{CO}_2$ in the gas samples in the Jimo geothermal system. Sedimentary-derived carbon (S) with $\text{CO}_2/\text{He}^{3\text{He}} = 1 \times 10^{13}$ and $\delta^{13}\text{C} = -30 \pm 10\text{‰}$ and limestone carbon (L) with a $\text{CO}_2/\text{He}^{3\text{He}}$ ratio of 1×10^{13} and $\delta^{13}\text{C}$ level of $0 \pm 2\text{‰}$ (Sano and Marty, 1995; Ray et al., 2009). (B) N_2/He vs. $^{20}\text{Ne}/\text{He}$ diagram. The N_2/He ratios for the air, mantle and sediment are 1,489,000 (Ozima and Podosek, 2002; Zimmer et al., 2004), 150 (Marty and Zimmerman, 1999) and 10,500 (Fischer et al., 2002), respectively. The $^{20}\text{Ne}/\text{He}$ ratios for the air, mantle and sediment are 3.145, 0.001 and 0.001 (Sano and Wakita, 1985), respectively. S-N input: sedimentary nitrogen input.

$\delta^{13}\text{C}_{\text{CH}_4}$ values disagree with the isotope evolution trend of migrated gas by diffusion or the residual gas by diffusion, microbial or abiogenic oxidization (Fig. 6B). The decreasing trends in $\delta\text{D}_{\text{CH}_4}$ and $\delta^{13}\text{C}_{\text{CH}_4}$ but increased isotope fractionation factor of carbon between CH_4 and CO_2 ($\alpha^{13}\text{C}_{\text{CH}_4-\text{CO}_2} = 0.978\text{--}0.987$) (Table 2) reflect that the CH_4 from the shallow aquifer may be produced primarily by acetate fermentation, which is characterized by $\delta^{13}\text{C}$, δD and $\alpha^{13}\text{C}_{\text{CH}_4-\text{CO}_2}$ values of -65 to -50‰ , -400 to -250‰ (Whiticar et al., 1986) and higher than 0.95 (Clark and Fritz, 1997), respectively. This inference is also consistent with the results of previous studies showing that acetate fermentation is attributed to the $> 70\%$ methanogenesis that takes place in a freshwater environment (Sherwood-Lollar et al., 1988; Whiticar et al., 1986).

Above all, combined with widely distributed organic-rich sediments (e.g., lacustrine silty sediment) (Liu et al., 2010), the microbial gas (CH_4 , CO_2 , H_2) in the shallow aquifer is likely produced in two steps, (1) the decomposition of the complex organic matter into simple molecules such as acetate (CH_3COOH), CO_2 and H_2 :



and (2) further production of CH_4 by acetate fermentation (Clark and Fritz, 1997; McMahon and Chapelle, 1991).



5.2.2. Evolutionary path II

The gas from HW06 in the western part is characterized by an abnormally high H_2/CH_4 ratio (46). The similar δD value (-740‰) relative to the other gas samples (-774 to -709‰) indicates that the extra H_2 may also be of microbial origin. The mixing with organic CO_2 is similar to that of other samples in the western part (Fig. 8A). However, the high $\text{H}_2/\text{He}^{3\text{He}}$, $\text{N}_2/\text{He}^{3\text{He}}$, $\text{CO}_2/\text{He}^{3\text{He}}$ and low $\text{CH}_4/\text{He}^{3\text{He}}$ ratios for HW06 indicate that the extra gas generation processes are slightly different from those of shallow fresh environments, which is confirmed by the evolution of N_2 . Notably, the gas samples, except that from HW06, plot along the air-mantle mixing curve (Fig. 8B), indicating that different levels of atmospheric N_2 have been added in as the geothermal fluids flow from the central to the western and eastern parts. By contrast, the gas from HW06 deviates from the mixing line towards the sediment end-member, reflecting a sedimentary nitrogen input. The deviation caused by sedimentary nitrogen input can also be found in the $\text{N}_2\text{-He-Ar}$ plot (Fig. 2), in which higher N_2/He in arcs than MORB are

due to additional nitrogen from marine sediments (Zimmer et al., 2004; Fiebig et al., 2004; Fischer et al., 2002).

With reference to the paleogeographic environment, the study area has experienced a Holocene transgression (X.J. Wang, 2018) with unevenly distributed marine sediments (Luan et al., 2007). The mixture of fossil marine constituents in HW06 has been identified by the geochemical signatures of geothermal water that is rich in bromine (Br) and iodine (I) (Hao et al., 2019). Therefore, the extra gas (biogenic H_2 and CO_2 , sedimentary input N_2) is likely derived from the fossil residual marine environment and is produced by the microbiological decomposition of organic matter (CO_2 , H_2) accompanied by nitrate reduction to nitrogen or the degradation of nitrogen-bearing organic matter (Kotarba et al., 2014; Mingram et al., 2005; Clark and Fritz, 1997; Sano et al., 1993), which need to be further identified by nitrogen isotope ratios. The low $\text{CH}_4/\text{He}^{3\text{He}}$ ratio indicates that methanogenesis is hindered. According to previous studies, the dominant methanogenesis process in a marine environment is CO_2 reduction by H_2 : $\text{CO}_2 + 4\text{H}_2 \rightarrow \text{CH}_4 + 2\text{H}_2\text{O}$ (Chuang et al., 2019; Whiticar et al., 1986; Clark and Fritz, 1997), rather than acetate fermentation (Koyama, 1963). The inhibition of methanogenesis may result from the fact that the primary terminal electron-accepting reactions during H_2 oxidation are nitrate reduction (considering the increase in $\text{N}_2/\text{He}^{3\text{He}}$) or other reactions with higher redox potentials (e.g., Fe^{III} , Mn^{IV} and sulfate reduction) rather than CO_2 reduction (Chuang et al., 2019; Lin et al., 2012; Lovley and Goodwin, 1988). This explanation is reasonable in the perspective of the evolutionary pattern of the H_2 hydrogen isotopes from HW06 with a marine end-member characterized by δD values of -814 to -763‰ (Krichevsky et al., 1961) and high H_2/CH_4 ratios. As shown in Fig. 9, the gas from HW06 has undergone mixing with microbial H_2 from shallow freshwater facies and marine facies.

The high concentration of H_2 with a low CH_4 concentration in the study area indicates that the extra H_2 is formed in the overlying brown lacustrine silty sediments and marine sediments with insignificant methanogenic activity or other hydrogen oxidation reactions (McMahon and Chapelle, 1991; Stevens and McKinley, 1995), which causes the consumption of H_2 to be far lower than the fermentative capacity.

5.2.3. Evolutionary path III

The CO_2 concentration of the HW09 in the eastern part reaches up to 1.89 vol%, which is 7–47 times higher than those in the western and central parts.

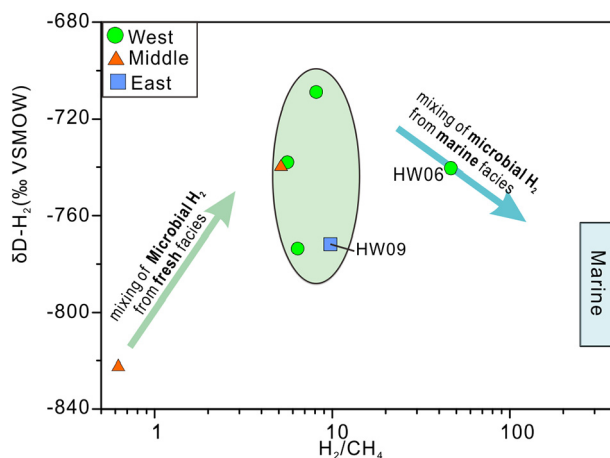


Fig. 9. $\delta\text{D-H}_2$ vs. H_2/CH_4 . Marine: the marine end-member with a δD value of -814 to $-763\text{\textperthousand}$ (Krichevsky et al., 1961) and an inferred high H_2/CH_4 ratio of > 46.5 .

The increases in CH_4/He , H_2/He and $\delta\text{D-H}_2$ similar to that in other samples in the western part indicate that the microbial CH_4 and H_2 produced in the shallow lacustrine silty clay have also been added to the HW09 sample (Fig. 7 and Fig. 9). Although it is more likely that organic CO_2 produced by the same process as microbial CH_4 and H_2 has been added to HW09 sample, the synchronous increases in CO_2/He and $\delta^{13}\text{C}$ (Fig. 8A) indicate that the addition of inorganic carbon is the primary reason for the high CO_2 . Combined with the acidic environment ($\text{pH} = 4.19$) in sample HW09 and the carbonates (calcite, dolomite) in the sediments and sandstone (Hao et al., 2019; Luan et al., 2007), carbonate dissolution accounts for the high CO_2 concentration and $\delta^{13}\text{C}$ value in the eastern part.

5.3. Process for the biotic methane with abiotic signatures

According to the $\delta^{13}\text{C}$ and δD values for CH_4 , gas samples from HW06 and HW09 deviate from those in the biotic zone and exhibit abiotic isotope signatures (Fig. 6B). As previously mentioned, CH_4 from a deep reservoir (thermogenic CH_4) and shallow environment (microbial CH_4) are both of biogenic origin. Therefore, the abiotic isotope signatures of CH_4 may be attributed to other secondary processes instead of simply mixing.

In contrast to the decreasing trends in the $\delta^{13}\text{C}$ and δD values from the central to the western parts, the CH_4 in HW09 is characterized by increased $\delta^{13}\text{C}$ and decreased δD values (Fig. 6B). Typical secondary processes such as microbial oxidation (Coleman et al., 1981; Kinnaman et al., 2007), abiogenic oxidation (Etiope et al., 2011a); and isotope fractionation by diffusion (Etiope and Sherwood-Lollar, 2013), cannot account for the variations in the $\delta^{13}\text{C}$ and δD signatures since these processes usually cause enrichment in both $\delta^{13}\text{C}$ and δD for the residual gas or decrease of $\delta^{13}\text{C}$ and increase of δD for the diffused gas (Fig. 6B). The δD value for CH_4 in HW09 ($-257\text{\textperthousand}$) is consistent with those of the other samples (-282 to $-221\text{\textperthousand}$), which indicates that the secondary processes have induced ^{13}C enrichment only without changing the hydrogen isotope. The isotope exchange between CH_4 and CO_2 is a common process that can impact the carbon isotope composition of methane (Arnórsson, 2000). At a certain temperature, the initial isotope difference and gas ratio are important factors influencing the isotope exchange reaction (Clark and Fritz, 1997). As discussed above, calcite dissolution causes a very large inorganic CO_2 concentration with a high $\delta^{13}\text{C}$ value to be added to the system, which not only results in an extremely low CH_4/CO_2 ratio (0.4) that is one to two orders of magnitude lower than those of the other samples (4.4–95.0) (Fig. 10A) but also increases the difference in the $\delta^{13}\text{C}$ between CO_2 and CH_4 . In this case, it is most likely that the measurable shift in CH_4 is caused by isotope

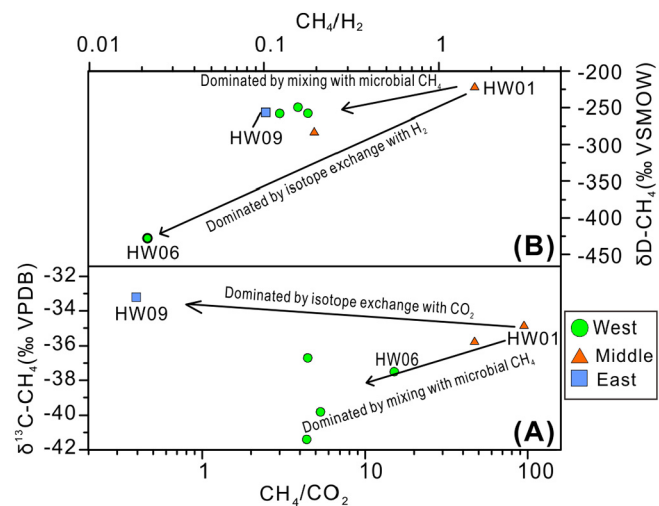


Fig. 10. (A) $\delta\text{D-CH}_4$ vs. CH_4/H_2 and (B) $\delta\text{C-CH}_4$ vs. CH_4/CO_2 .

exchange. Therefore, the increase in the $\delta^{13}\text{C}$ value for the CH_4 in HW06 is likely to be attributed to the isotope exchange between CH_4 and CO_2 with a high $\delta^{13}\text{C}$ value and a low CH_4/CO_2 ratio.

A similar abnormal phenomenon also occurs for sample HW06. The carbon isotope ratio for CH_4 in HW06 is of a typical microbial origin; however, the extremely negative δD value ($-427.8\text{\textperthousand}$) is an abiotic signature (Fig. 6B). The gas from HW06 is also characterized by the highest H_2 concentration (12.5%) and the lowest CH_4/H_2 ratio (0.02) (Fig. 10B), which will significantly shift the deuterium ratio for CH_4 at such a low CH_4/H_2 ratio without changing the carbon isotope ratios. Therefore, the δD level of CH_4 is evolving towards the low δD level of H_2 ($-740\text{\textperthousand}$) by isotope exchange.

5.4. Conceptual model of gas evolution

By integrating the topographic features, geological conditions and hydrochemical and isotope signatures, a conceptual model of gas evolution in the study area is tentatively proposed (Fig. 11). Meteoric water from the surrounding mountains infiltrates the subsurface through fractures. The infiltrated water and basalt interaction through the reduction of water and oxidation of Fe^{II} in pyroxene and olivine produces H_2 under near-surface conditions in the Bamudi Formation of the Qingshan Group located 2 km northwest of the geothermal system, which then migrates into the sandstone-hosted geothermal reservoir via the dominant NW extensional Dongkuang-Shuibo fault and mixes with the CH_4 and CO_2 generated by thermal decomposition of organic material in the sandstone. The mixed deep gases rise along the conduits formed by the crossing of the NE and NW faults to the shallow aquifers. Subsequently, the deep-origin gases mix with a mass of microbial H_2 , CH_4 , and CO_2 produced by microbial fermentation processes in shallow fresh sediments as geothermal fluids flow from the central to the western and eastern parts. In addition, the extra biological H_2 , CO_2 and sediment-derived N_2 from the fossil residual marine sediments and inorganic CO_2 produced by carbonate dissolution are added to the gases in HW06 and HW09, respectively.

6. Conclusions

The Jimo geothermal gas is a rare example that illustrates how geochemical processes can generate extreme concentrations and isotope composition of gases. The abnormally high H_2 concentrations of 2.4 to 12.5 vol% with very depleted $\delta\text{D-H}_2$ values of -709 to $-822\text{\textperthousand}$ and the dramatic variations are closely related to the complicated geological environment of basalt, sandstone, residual fossil marine sediments, and organic-rich nonmarine sediments.

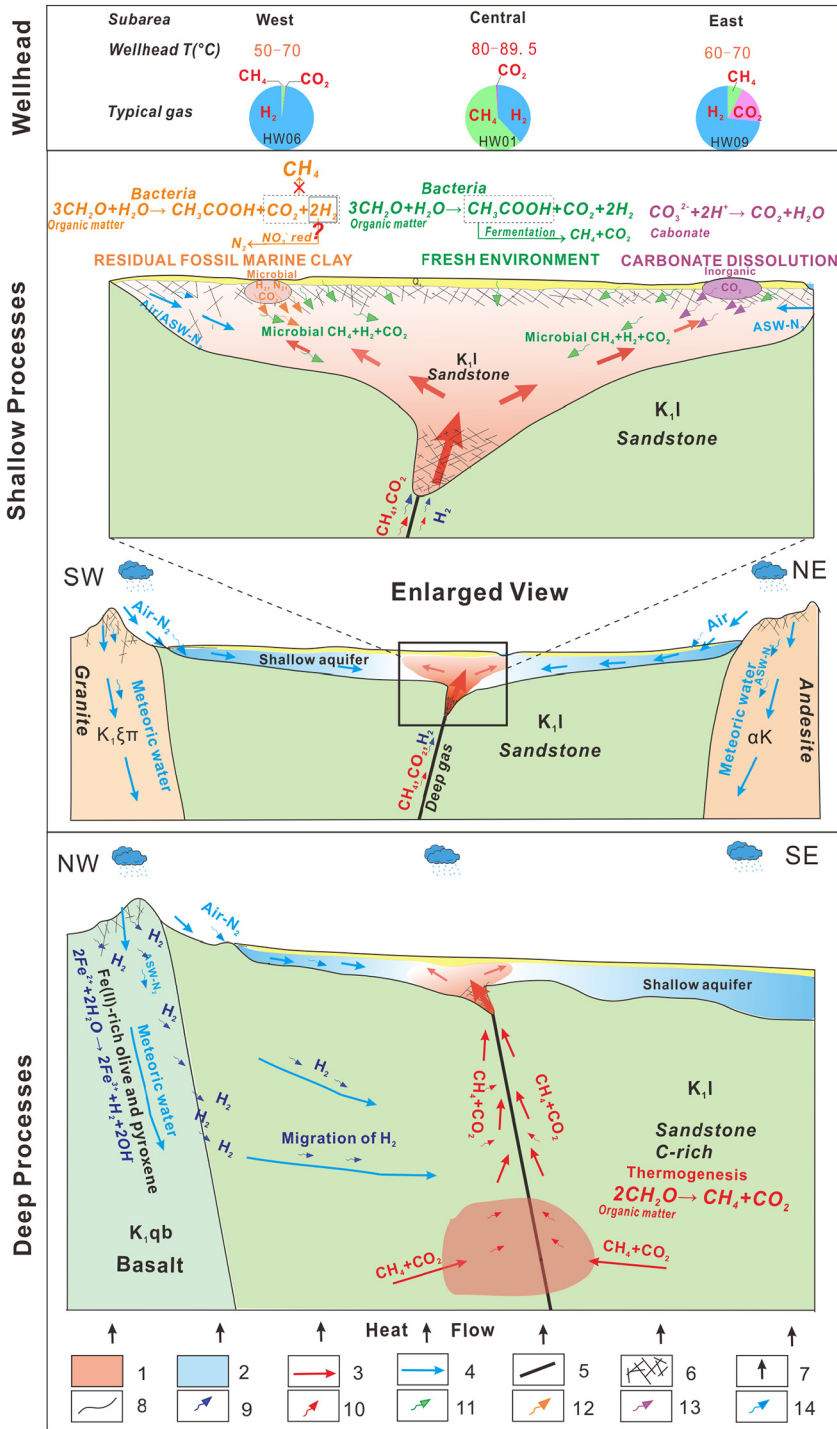


Fig. 11. A conceptual model of different gas generation and evolution mechanisms: (A) geothermal water temperature measured at the wellhead and gas composition of typical samples in each part; (B) mixing of gases from shallow environments as geothermal water flows from the central to the western and eastern parts; and (C) deep-seated gas generation and migration. Explanation: (1) geothermal reservoir; (2) fresh groundwater aquifer; (3) geothermal fluids flow direction; (4) meteoric water/groundwater flow direction; (5) fault; (6) permeable fracture zone; (7) heat flow; (8) boundary between different rocks; (9) abiotic H₂ generation by water reduction and Fe^{II}-rich pyroxene and olivine (serpentinitization); (10) thermogenic gas (CH₄ and CO₂); (11) microbial gas from lacustrine silty clay (H₂, CH₄, CO₂); (12) microbial gas from residual marine clay (H₂, CO₂, N₂); (13) inorganic CO₂ by carbonate dissolution; and (14) Air/ASW gas (N₂) (see 5.4 for detailed explanation).

- (1) By integrated chemical and isotope signatures of H₂ and associated other gas (noble gas, CH₄ and CO₂), geological and hydrogeological conditions, the most likely possibility for deep-origin H₂ generation is that H₂ is allochthonous and not formed in sandstone, but in the basalt through water reduction and the oxidation of Fe^{II}-rich pyroxene and olivine (serpentinitization) under near-surface conditions and has migrated into sandstone afterwards. By contrast, the deep-origin CH₄ is primarily generated by the thermal decomposition of organic materials in the sandstone.
- (2) A large amount of microbial H₂ is suggested to be produced in shallow fresh sediments and locally residual fossil marine facies by different evolutionary mechanisms. In lacustrine silty sediments,

the decomposition of organic matter and further acetate fermentation have produced excess H₂, CH₄ and CO₂. However, in locally residual marine sediments, the microbiological decomposition of organic matter accompanied by the reduction of nitrate to nitrogen or the degradation of nitrogen-bearing organic matter without methanogenesis has generated a considerable amount of H₂, N₂ and CO₂. The temperature predicted based on the H₂O-H₂ and CH₄-H₂O deuterium equilibria is approximately 40 °C lower than the well-head temperature measured on the average due to the mixing of shallow biogenic gases.

- (3) The biotic CH₄ affected by isotope exchange at a high H₂/CH₄ or CO₂/CH₄ ratio presents an isotope signature in the range of abiotic

- gases, suggesting that deuterium and carbon isotope signatures in methane should be used with caution to identify genetic origin of methane.
- (4) A data compilation of published hydrogen isotope ratios of H₂ produced by different mechanisms in various geological environment and experimental conditions has been systematically collected for the first time. The hydrogen isotope ratio pattern may provide a useful initial tool to restrict the dominant origin of H₂. However it is only a preliminary reference, and the integrated geochemical methods based on the concentration and isotope composition of associated gases, waters and a detailed knowledge of the geologic and hydrogeological conditions is necessary to confirm the genetic origins of H₂ and the post-genetic alteration processes.

These conclusions are still preliminary. And further experimental and numerical researches in quantification of the hydrogen isotope fractionation caused by gas migration, and the influence factors for consumption of H₂ by microorganisms are required to improve our understanding of these processes. And it is also necessary to look for other potential mechanisms.

Author contributions

Z. P. initiated and designed the study. Y. H., J. T. and Y. C. conducted the field work. Y. H., J. T., Z. L., L. L. and L. X. performed the geochemical and stable isotope analyses. Y. H. and Z. P. interpreted the data and wrote the manuscript. All of the authors contributed to the interpretation of the data and provided significant inputs into the final manuscript.

Funding

This work was supported by the National Natural Science Foundation of China (NSFC Grant 41877209) and the Jimo Thermal Power Plant Company.

Declaration of competing interest

The authors have no conflicts of interest to declare.

Acknowledgments

We gratefully acknowledge Chunhui Cao from the Lanzhou Center for Oil and Gas Resources, Institute of Geology and Geophysics, Chinese Academy of Sciences for their analyses of the gas compositions and He-Ne isotopes. Constructive comments by two anonymous reviewers, as well as the effort of the editors, are gratefully appreciated.

Appendix A. Supplementary data

Supplementary data to this article can be found online at <https://doi.org/10.1016/j.chemgeo.2020.119477>.

References

- Abrajano, T.A., Sturchio, N.C., Bohlke, J.K., Lyon, G.L., Poreda, R., Stevens, C., 1988. Methane-hydrogen gas seeps, Zambales Ophiolite, Philippines: deep or shallow origin? *Chem. Geol.* 71 (1–3), 211–222. [https://doi.org/10.1016/0009-2541\(88\)90116-7](https://doi.org/10.1016/0009-2541(88)90116-7).
- Amend, J.P., Shock, E.L., 2001. Energetics of overall metabolic reactions of thermophilic and hyperthermophilic Archaea and Bacteria. *FEMS Microbiol. Rev.* 25, 175–243.
- Arnason, B., 1977. The hydrogen-water isotope thermometer applied to geothermal areas in Iceland. *Geothermics* 5, 75–80.
- Arnason, B., Sigurgeirsson, T., 1968. Deuterium content of water vapor and hydrogen in volcanic gas at Surtsey, Iceland. *Geochim. Cosmochim. Acta* 32, 807–813.
- Arnórsson, S., 2000. Isotopic and Chemical Techniques in Geothermal Exploration, Development and Use. IAEA, Vienna.
- Balabane, M., Galimov, E., Hermann, M., Letolle, R., 1987. Hydrogen and carbon isotope fractionation during experimental production of bacterial methane. *Org. Geochem.* 11, 115–119.
- Blair, C.C., D'Hondt, S., Spivack, A.J., Kingsley, R.H., 2007. Radiolytic Hydrogen and Microbial Respiration in Subsurface Sediments. *Astrobiology* 7 (6), 951–970.
- Bottinga, Y., 1969. Calculated fractionation factors for carbon and hydrogen isotope exchange in the system calcite-carbon dioxide-graphite-methane-hydrogen-water vapor. *Geochim. Cosmochim. Acta* 33, 49–64.
- Bradley, A.S., Summons, R.E., 2010. Multiple origins of methane at the Lost City hydrothermal field. *Earth Planet. Sci. Lett.* 294, 34–41.
- Chuang, P.C., Yang, T.F., Wallmann, K., Matsumoto, R., Hua, C.Y., Chen, H.W., Lin, S., Sun, C.H., Li, H.C., Wang, Y., Dale, A.W., 2019. Carbon isotope exchange during anaerobic oxidation of methane (AOM) in sediments of the northeastern South China Sea. *Geochim. Cosmochim. Acta* 246, 138–155.
- Clark, I.D., Fritz, P., 1997. Environmental Isotopes in Hydrogeology. Lewis Publishers, Boca Raton.
- Coleman, D.D., Risatti, J.B., Schoell, M., 1981. Fractionation of carbon and hydrogen isotopes by methane oxidising bacteria. *Geochim. Cosmochim. Acta* 45, 1033–1037.
- Coveney, R.M.J., Goebel, E.D., Zeller, E.J., Dreschhoff, G.A.M., Angino, E.E., 1987. Serpentization and origin of hydrogen gas in Kansas. *AAPG Bull.* 71, 39–48.
- Craig, H., Lupton, J.E., Horibe, Y., 1978. A mantle helium component in circum Pacific volcanic glasses: Hakone, the Marianas and Mt. Lassen. In: Alexander, E.C., Ozima, M. (Eds.), *Terrestrial Rare Gases*. Japan Science Society Press, Tokyo, pp. 3–16.
- Des Marais, D.J., Donchin, J.H., Nehring, N.L., Truesdell, A.H., 1981. Molecular carbon isotopic evidence for the origin of geothermal hydrocarbons. *Nature* 292, 826–828.
- Duchkov, A.D., Rychkova, K.M., Lebedev, V.I., Kamenskii, I.L., Sokolova, L.S., 2010. Estimation of heat flow in Tuva from data on helium isotopes in thermal mineral springs. *Russ. Geol. Geophys.* 51 (2), 209–219.
- Etiöpe, G., Sherwood-Lollar, B., 2013. Abiotic methane on Earth. *Rev. Geophys.* 51, 276–299.
- Etiöpe, G., Baciu, C., Schoell, M., 2011a. Extreme methane deuterium, nitrogen and helium enrichment in natural gas from the Homorod seep (Romania). *Chem. Geol.* 280, 89–96. <https://doi.org/10.1016/j.chemgeo.2010.10.019>.
- Etiöpe, G., Schoell, M., Hosgormez, H., 2011b. Abiotic methane flux from the Chimaera seep and Tekirova ophiolites (Turkey): understanding gas exhalation from low temperature serpentization and implications for Mars. *Earth Planet. Sci. Lett.* 310 (1–2), 96–104. <https://doi.org/10.1016/j.epsl.2011.08.001>.
- Fan, W.M., Guo, F., Wang, Y.J., Lin, G., Zhang, M., 2001. Post-orogenic bimodal volcanism along the Sulu orogenic belt in eastern China. *Physics and Chemistry of the Earth (A)* 26, 733–746.
- Feldbusch, E., Wiersberg, T., Zimmer, M., Regenspurg, S., 2018. Origin of gases from the geothermal reservoir Groß Schönebeck (North German Basin). *Geothermics* 71, 357–368. <https://doi.org/10.1016/j.geothermics.2017.09.007>.
- Feng, M., Song, H., Yang, Q., Liu, J., 2016. Characteristics of dissolved gases and trace element in geothermal waters in Jiangsu and their tracing significance. *HYDROGEOLGY & ENGINEERING GEOLOGY* 43 (1), 164–170.
- Fiebig, J., Chiodini, G., Caliro, S., Rizzo, A., Spangenberg, J., Hunziker, J.C., 2004. Chemical and isotopic equilibrium between CO₂ and CH₄ in fumarolic gas discharges: generation of CH₄ in arc magmatic-hydrothermal systems. *Geochim. Cosmochim. Acta* 68 (10), 2321–2334.
- Fischer, T.P., Hilton, D.R., Zimmer, M.M., Shaw, A.M., Sharp, Z.D., Walker, J.A., 2002. Subduction and recycling of nitrogen along the middle American margin. *Science* 297, 1154–1157.
- Fritz, P., Clark, I.D., Fontes, J.C., Whiticar, M.J., Faber, E., 1992. Deuterium and ¹³C evidence for low temperature production of hydrogen and methane in a highly alkaline groundwater environment in Oman. In: Kharaka, Y.K., Maest, A.S. (Eds.), *Proceedings of the 7th International Symposium on Water-Rock Interaction; Volume 1, Low Temperature Environments. Proceedings—International Symposium on Water-Rock Interaction, International Association of Geochemistry and Cosmochemistry and Alberta Research Council, Sub-Group on Water-Rock Interaction*, Edmonton, AB, International, pp. 793–796.
- Frost, B.R., Beard, J.S., 2007. On silica activity and serpentization. *J. Petrol.* 48, 1351–1368.
- Fu, Q., Sherwood Lollar, B., Horita, J., Lacrampe-Couloume, G., Seyfried, W.E., 2007. Abiotic formation of hydrocarbons under hydrothermal conditions: constraints from chemical and isotope data. *Geochim. Cosmochim. Acta* 71, 1982–1998.
- Giggenbach, W.F., 1992. Isotopic shifts in waters from geothermal and volcanic systems along convergent plate boundaries and their origin. *Earth Planet. Sci. Lett.* 113, 495–510.
- Giggenbach, W.F., Poreda, R.J., 1993. Helium isotopic and chemical composition of gases from volcanic-hydrothermal systems in the Philippines. *Geothermics* 22, 369–380.
- Gunter, B.D., Musgrave, B.C., 1971. New evidence on the origin of methane in hydrothermal gases. *Geochim. Cosmochim. Acta* 35, 113–118.
- Hao, Y., Pang, Z., Huang, T., Kong, Y., Tian, J., Wang, Y., 2019. Synthesis of geochemical techniques to identify the origin and multistage evolution of saline water in a complex geothermal system. *E3S Web of Conferences* 98, 08005. <https://doi.org/10.1051/e3sconf/2019980005>.
- Hoehler, T.M., Alperin, M.J., Albert, D.B., Martens, C.S., 1998. Thermodynamic control on hydrogen concentrations in anoxic sediments. *Geochim. Cosmochim. Acta* 62 (10), 1745–1756.
- Horibe, Y., Craig, H., 1995. D/H fractionation in the system methane–hydrogen–water. *Geochim. Cosmochim. Acta* 59, 5209–5217.
- Huang, G., Sun, J., 2007. Composing Characteristic of Groundwater Hydrogen and Oxygen Isotopes in Northern China Plains and Basins. *Groundwater* 29 (4), 30–31.
- Ji, Q., 2017. On the Cretaceous stratigraphic framework and the Cretaceous-Paleogene boundary of Eastern Shandong Province. *J. Geol.* 4 (1), 1–25 (in Chinese with English abstract).
- Karakus, H., 2015. Helium and carbon isotope composition of gas discharges in the Simav

- K., Hongoh, Y., Kawachi, K., Omori, S., Yamada, K., Yoshida, N., Maruyama, S., 2014. Origin of methane in serpentinite-hosted hydrothermal systems: the CH₄-H₂-H₂O hydrogen isotope systematics of the Hakuba Happo hot spring. *Earth Planet. Sci. Lett.* 386, 112–125.
- Sugisaki, R., Ido, M., Takeda, H., Isobe, Y., Hayashi, Y., Nakamura, N., Satake, H., Mizutani, Y., 1983. Origin of hydrogen and carbon dioxide in fault gases and its relation to fault activity. *J. Geol.* 91 (3), 239–258.
- Tao, S., Liu, D., 2000. Geothermal field characteristics of TanLu fault zone and its neighbouring regions, thermal spring genesis and its composition. *NATUR. GAS IND.* 20 (6), 42–47 (In Chinese with English abstract).
- Taran, Y.A., Pilipenko, V.P., Rozhkov, A.M., Vakin, E.A., 1992. A geochemical model for fumaroles of the Mutnovsky Volcano, Kamchatka, USSR. *J. Volcanol. Geotherm. Res.* 49, 269–283.
- Taran, Y.A., Varley, N.R., Inguaggiato, S., Cienfuegos, E., 2010. Geochemistry of H₂- and CH₄-enriched hydrothermal fluids of Socorro Island, Revillagigedo Archipelago, Mexico. Evidence for serpentinization and abiogenic methane. *Geofluids* 10, 542–555.
- Tardani, D., Reich, M., Rouleau, E., Takahata, N., Sano, Y., Pérez-Flores, P., Sánchez-Alfaro, P., Cembrano, J., Arancibia, G., 2016. Exploring the structural controls on helium, nitrogen and carbon isotope signatures in hydrothermal fluids along an intra-arc fault system. *Geochim. Cosmochim. Acta* 184, 193–211. <https://doi.org/10.1016/j.gca.2016.04.031>.
- Tian, J., Pang, Z., Guo, Q., Wang, Y., Li, J., Huang, T., Kong, Y., 2018. Geochemistry of geothermal fluids with implications on the sources of water and heat recharge to the Rekeng high-temperature geothermal system in the Eastern Himalayan Syntax. *Geothermics* 74, 92–105.
- Vacquand, C., Deville, E., Beaumont, V., Guyot, F., Sissmann, O., Pillot, D., Arcilla, C., Prinzhofer, A., 2018. Reduced gas seepages in ophiolitic complexes: evidences for multiple origins of the H₂-CH₄-N₂ gas mixtures. *Geochim. Cosmochim. Acta* 223, 437–461.
- Wan, Y., Zhang, Q., 1987. Study on the origin of the warm springs in the wenquan town, Jimo country, Qingdao. *Journal of Oceanography of Huanghai & Bohai Seas* 5 (3), 27–32.
- Wang, X., 2018a. Formation Conditions and Hydrogeochemical Characteristics of the Geothermal Water in Typical Coastal Geothermal Field With Deep Faults, Guangdong Province. Ph. D. thesis. China University of Geosciences.
- Wang, X.J., 2018b. A Study of the Characteristics and Genesis of the Hot Springs in the Western Shandong Peninsula. Master thesis. China University of Geosciences, Beijing.
- Wang, D., Eoghan, P., Reeves, E.P., McDermott, J.M., Seewald, J.S., Ono, S., 2018. Clumped isotopologue constraints on the origin of methane at seafloor hot springs. *Geochim. Cosmochim. Acta* 223, 141–158.
- Wetzel, L.R., Shock, E.L., 2000. Distinguishing ultramafic- from basalt-hosted submarine hydrothermal systems by comparing calculated vent fluid compositions. *J. Geophys. Res.* 104 (B4), 10439–10460.
- Whiticar, M.J., Faber, E., Schoell, M., 1986. Biogenic methane formation in marine and freshwater environments: CO₂ reduction vs. acetate fermentation-isotope evidence. *Geochim. Cosmochim. Acta* 50, 693–709.
- Yuan, J., 2013. Hydrogeochemistry of the Geothermal Systems in Coastal Areas of Guangdong Province, South China. Ph. D. thesis. China University of Geosciences.
- Zhai, S., 2003. Formation and Evolution of Jiaolai Basin and Formation Condition of Combination Gas. Ph. D. thesis. Guangzhou Institute of Geochemistry, Chinese Academy of Science.
- Zhang, H., Sun, M., 2002. Geochemistry of Mesozoic Basalts and Mafic Dikes, Southeastern North China Craton, and Tectonic Implications. *Int. Geol. Rev.* 44 (4), 370–382. <https://doi.org/10.2747/0020-6814.44.4.370>.
- Zhang, T., Zhang, Y.Q., 2008. Late Mesozoic tectono-magmatic evolution history of the Jiaobei Uplift, Shandong Peninsula. *Acta Geol. Sin.* 82, 1210–1218 (in Chinese with English abstract).
- Zhang, Z., Shao, S., Chen, Y., Wei, J., Shi, D., Shi, J., 1999. Geological Environment Evolution Since Late Pleistocene in Northern China and Prediction of Future Living and Surviving Environment Change Trend. *Geology Press, Beijing*.
- Zhang, Y., Li, J., Zhang, T., Yuan, J., 2007. Late Mesozoic kinematic history of the Muping-Jimo fault zone in Jiaodong peninsula, Shandong Province, East China. *Geol. Rev.* 53 (3), 289–300 (in Chinese with English abstract).
- Zhang, L., Wang, C., Cao, K., Wang, Q., Tan, J., 2016. High elevation of Jiaolai Basin during the Late Cretaceous: implication for the coastal mountains along the East Asian margin. *Earth Planet. Sci. Lett.* 456 (15), 112–113.
- Zhang, P., Kuang, H., Liu, Y., Meng, Z., Peng, N., Huan Xu, H., 2019. Sedimentary characteristics and provenance of the basal conglomerate of the Late Jurassic-Early Cretaceous Jiaolai Basin, eastern China and their implications for the uplift of the Sulu Orogenic Belt. *Int. Geol. Rev.* 61 (5), 521–538. <https://doi.org/10.1080/00206814.2018.1437786>.
- Zhou, Y., Ji, Y., Zhang, S., Wan, L., 2016. Controls on reservoir quality of Lower Cretaceous tight sandstones in the Laiyang Sag, Jiaolai Basin, Eastern China: integrated sedimentologic, diagenetic and microfracturing data. *Mar. Pet. Geol.* 76, 26–50.
- Zhou, X., Liu, L., Chen, Z., Cui, Y., Du, J., 2017. Gas geochemistry of the hot spring in the Litang fault zone, Southeast Tibetan Plateau. *Appl. Geochem.* 79, 17–26.
- Zhu, X., Ren, T., Yang, S., Hou, J., 2012. Characteristics of volcanic rocks and its internal sandstone of Bamudi formation in the Jimo Area of Qingdao City. *Land and Resources in Shandong Province* 28 (10), 21–24 (in Chinese with English abstract).
- Zimmer, M.M., Fischer, T.P., Hilton, D.R., Alvarado, G.E., Sharp, Z.D., Walker, J.A., 2004. Nitrogen systematics and gas fluxes of subduction zones: insights from Costa Rica arc volatiles. *Geochem. Geophys. Geosyst.* 5, Q05J11.
- Zolotarev, B.P., Voytov, G.I., Sarkisyan, I.S., Cherevichnaya, L.E., 1978. Gases in basaltoid rocks of the Mid-Atlantic Ridge, as shown by data from the 45th voyage of the Glomar Challenger. *Akademiya Nauk SSSR Doklady* 243, 207–210.